Computational Materials Science 145 (2018) 263–279

Contents lists available at ScienceDirect

Computational Materials Science

journal homepage: www.elsevier.com/locate/commatsci

Insight into the C—C chain growth in Fischer-Tropsch synthesis on HCP Co(10-10) surface: The effect of crystal facets on the preferred mechanism

Riguang Zhang [a,b], Li Kang [a], Hongxia Liu [a], Leilei He [b], Baojun Wang [a,*]

[a] Key Laboratory of Coal Science and Technology of Ministry of Education and Shanxi Province, Taiyuan University of Technology, Taiyuan 030024, Shanxi, PR China
[b] Department of Chemical and Petroleum Engineering, The University of Wyoming, Laramie, WY 82071, USA

ARTICLE INFO

Article history:
Received 10 August 2017
Received in revised form 20 December 2017
Accepted 3 January 2018

Keywords:
Fischer-Tropsch synthesis
Co(10-10)
C—C chaingrowth
Preferred mechanism
Density functional theory

ABSTRACT

Spin-polarized DFT calculations are performed to probe into the preferred mechanism of C—C chain growth in Fischer-Tropsch synthesis on HCP Co(10-10) with the higher surface area exposed. The effect of HCP Co crystal facets on the preferred mechanism of C—C chain growth is identified among carbide mechanism and C(H)O mechanism in the processes of C_1 to C_4 hydrocarbons. CH_2 is the most favored CH_x monomer. The C_2 hydrocarbon is dominantly formed via carbide mechanism, and CH_3CH_2 is the most favored C_2 hydrocarbon. Subsequently, the most favored C_3 hydrocarbon, $CH_3CH_2CH_2$, is formed via carbide mechanism of CH_3CH_2 coupling with CH_2. Further, the most favored C_4 hydrocarbon, $CH_3CH_2CH_2CH_2$, is formed via carbide mechanism of $CH_3CH_2CH_2$ coupling with CH_2. Thus, the preferred mechanism of C—C chain growth on Co(10-10) mainly focus on carbide mechanism instead of C(H)O insertion mechanism. The carbide mechanism is that RCH_2 coupling with CH_2 to $R'CH_2$ ($R'=RCH_2$), followed by coupling with CH_2 to $R''CH_2$($R''=R'CH_2$) can realized the C—C chain growth cycle to form higher hydrocarbons. Finally, the crystal facet of HCP Co catalyst affects the preferred mechanism of C—C chain growth, and Co(10-10) *via* carbide mechanism is more favorable than Co(0 0 0 1) *via* CHO insertion mechanism.

© 2018 Elsevier B.V. All rights reserved.

1. Introduction

Fischer-Tropsch synthesis (FTS) [1,2] can convert syngas (CO + H_2) to the products containing olefins, paraffin and small amounts of oxygenates [3–6]. FTS reaction can be catalyzed by certain transition metals Co, Fe, Ru and Ni. Among them, Co is the preferred catalyst for FTS due to its high activity and selectivity towards linear hydrocarbons, low activity for water-gas shift reaction, and more stable towards deactivation by water and relatively low cost [7–10].

Nowadays, several mechanisms are proposed for the formation of hydrocarbons in FTS reactions [11]. Carbide mechanism proposed by Fischer and Tropsch [12] claimed C_1 intermediates are formed by CO direct dissociation into C, followed its hydrogenation to CH_2, which acts as monomer to insert into the hydrocarbon chain to realize the C—C chain growth, this results are also confirmed by the experiment [13]. Meanwhile, CH_2 + CH coupling on Co(0 0 0 1) surface [14] exists. Cheng et al. [15,16] showed that CH_2 self-coupling is favored on the stepped Co(0 0 0 1), while CH self-coupling is favored on the flat Co(0 0 0 1); moreover, CH_2-like species (CH_3CH) coupling with CH_2 is also dominant on the stepped Co(0 0 0 1) [17]. On the other hand, CO/CHO insertion mechanism is also proposed, Pichler and Schulz [18] showed that the C—C chain growth occurs by CO insertion into RCH_2 to RCH_2CO, followed by its C—O bond scission on Co(0 0 0 1) surface. However, CO insertion into RCH_2 has the high barrier [19]; then, Masters et al. [20] and Zhuo et al. [19,21] proposed CO insertion into RCH for the C—C chain growth. Density functional theory (DFT) studies by Deng et al. [22] also show that C_2H_x is formed via CO insertion mechanism. Alternatively, CHO insertion into CH_x is also accepted as the C—C chain growth pathway [23–26], for example, CHO insertion into CH_2 is more favorable CO insertion for C—C chain growth on Co(0 0 0 1) [23].

As mentioned above, for Co catalyst, up to now, only Co(0 0 0 1) surface has been widely examined, however, few systematical comparisons between carbide mechanism and CO/CHO insertion mechanism are carried out over Co(0 0 0 1) surface, only carbide mechanism or CO/CHO insertion mechanism is separately discussed. Moreover, few studies about the C—C chain growth are

* Corresponding author.
E-mail addresses: wangbaojun@tyut.edu.cn, wbj@tyut.edu.cn (B. Wang).

https://doi.org/10.1016/j.commatsci.2018.01.013
0927-0256/© 2018 Elsevier B.V. All rights reserved.

reported over other Co surface. Thus, our recent DFT studies [27] have fully investigated and compared the C—C chain growth via carbide mechanism and CO/CHO insertion mechanism on Co(0 0 0 1) surface, suggesting that the C—C chain growth is realized by CHO insertion mechanism. Subsequently, a detailed C—C chain formation and growth mechanism for C_{2+} hydrocarbons in FTS reactions on Hcp Co(10-11) surface [28] are also investigated using DFT calculations together with microkinetic modeling, the proposed mechanism of C—C chain growth cycle is that the carbide mechanism with RCH_2CH_2 coupling with CH_2 to $R'CH_2CH_2$(R'=RCH_2). Thus, the mechanism of C—C chain growth in FTS reactions depends on Co crystal facets; in addition, previous studies show that the preferred mechanism of C—C chain growth in FTS reactions on Co catalyst is sensitive to Co crystal facets [14–17].

Given that the real Co catalyst consists of different crystal facets, probing into the preferred mechanism of C—C chain growth on different Co crystal facets can help us to obtain the effect of Co crystal facets on the preferred mechanism. However, up to now, except for above reported studies on Hcp Co(0 0 0 1) and Co(10-11) surfaces with the corresponding 18% and 35% of the total surface area exposed [27,28], few studies on Hcp Co(10-10) with the large 28% of the total surface area exposed [29] has been mentioned, which have become an obstruction for fully understanding the catalytic performance and the optimization of Co-based catalysts, as well as the development of detailed kinetics. Thus, it is significant to investigate the preferred mechanism of C—C chain growth on different Co crystal facets.

In this study, the mechanism of C—C chain growth for hydrocarbons formation on Hcp Co(10-10) surface in FTS reactions has been investigated using DFT calculations together with microkinetic modeling; both carbide mechanism and CO/CHO insertion mechanism are considered and compared to identify the preferred mechanism of C—C chain growth. The results are expected to obtain the preferred mechanism of C—C chain growth on Co(10-10) surface at a molecular level; then, comparisons with that on Co(0 0 0 1) and Co(10-11) surfaces can identify the effect of crystal facet on the preferred mechanism of C—C chain growth for hydrocarbons formation on Hcp Co catalyst, which would provide a clue for the catalyst design of the desirable FTS products by manipulating the crystal facets of Co catalyst using the well-defined preparation method.

2. Computational details

2.1. Computational methods

Periodic spin-polarized DFT calculations have been performed by using the Vienna Ab Initio Simulation Package (VASP) [30–32], the kinetic energy cutoff is 400 eV for a plane wave basis set. The electron-ion interaction is described by the projector augmented wave (PAW) method, and the generalized gradient approximation with Perdew-Burke-Ernzerhof exchange-correlation functional (GGA-PBE) is used for the exchange-correlation function [33]. A $5 \times 5 \times 1$ Monkhorst-Pack mesh *k*-point sampling within the Brillouin zone is used [34]. The optimization is thought to be converged when the total energy change between two consecutive steps are smaller than 5×10^{-6} eV/atom, and the forces change between two steps is smaller than 10^{-2} eV/Å.

The activation energy, all transition states (TS) are obtained using the climbing-image nudged elastic band method (CI-NEB) method [35,36]. The located TS have been optimized using the dimer method [37,38]. The structure of the TS is deemed converged when the forces acting on the atoms are all less than 0.05 eV/Å, and the structures is at a saddle point. The transition state is confirmed by the existence of only one imaginary frequency along the proper reaction coordinates.

For a given system, choosing a proper functional is the basis for obtaining the accurate calculation results. Teng et al. [39] showed that RPBE functional was more suitable for FTS reactions for Co surface. DFT studies by Liu et al. [40] showed that RPBE functional is more suitable to investigate surface O removal by H and CO on Co(0 0 0 1) surface. In this study, our result shows the optimized lattice constant are 2.49 and 2.51 Å using PBE and RPBE functional, which agree with the experiment value of 2.51 Å [41], and other calculated values of 2.51 Å [42] and 2.49 Å [19]. On the other hand, the adsorption energies, sites and key structure parameters for the most stable configurations of partial key adsorbed species involving in the C—C chain growth on Co(10-10) surface have been calculated by PBE and RPBE functional (see Table S1), indicating that the adsorption free energies have a certain difference obtained by PBE and RPBE functional, the values obtained by RPBE functional are slightly larger than that by PBE functional, while the trend of change are same; further, the activation free energy and reaction free energies of six reactions related to CH_2 and CH_3CH_2 (see Table S2) show that the favorable pathway obtained by PBE functional agrees with that by RPBE functional. Thus, RPBE and PBE functional can give the same conclusion, namely, PBE functional in this study is reliable for the studies of C—C chain growth on Co(10-10).

Given that the long-range dispersion corrections for van der Waals interaction may affect the calculated results, the DFT-D3 method [43,44] has been employed to test the effect of van der Waals interaction on the energetic, barrier and adsorption configuration in this study. DFT-D3 method allows for geometry optimization including van der Waals interactions at each optimization step using the VASP code, and it is not a correction of the energy after geometry optimization. Our test results (see Table S3) show that DFT and DFT-D3 calculations present the negligible differences for the adsorption energies of the species with the stronger adsorption ability; however, DFT and DFT-D3 calculations have the slight differences for the adsorption energies of the species with a weak physisorption. Moreover, DFT and DFT-D3 calculations present the negligible changes for the geometry of the stable adsorption configurations including the species with a stronger adsorption ability, as well as CH_4, C_2H_6 and C_3H_8 species with weak physisorption ability. Further, DFT and DFT-D3 calculations present the negligible differences for the activation and reaction energies of some key reactions involving in FTS on Co(10-10) (see Table S4). The reason may be that DFT-D3 methods only well describe the weak adsorption and the conformations of molecular cluster [45,46].

2.2. Surface model

Co exists in the form of two crystallographic structures, the hexagonal close packed (HCP) phase and the face-centered cubic (FCC) phase. Under the realistic FTS conditions, HCP Co phase is rich, and its exhibits a high CO conversion compared to FCC Co phase [47,48]. Moreover, when the temperature is above about 690 K, the phase transition from HCP Co to FCC Co occurs [49–51], suggesting that FCC Co phase cannot exist in FTS reactions due to the low temperature of about 473–623 K [8,52,53]. As a result, in this study, only HCP Co phase is considered.

The morphology of HCP Co is a dihedral-like shape with two close-packed (0001) facets [29], although (0001) surface has the very low surface energy, it covers only 18% of the total surface area exposed, and it shows a poor catalytic activity towards CO activation and conversion. Meanwhile, the open Co(10-11) and Co(10-10)-A facets with the higher surface energy dominate 35 and 28% of the total surface area exposed, respectively. However, Co(10-10)-A surface has lower surface energy than Co(10-11) surface [29], indicating that Co(10-10)-A surface area is easier to expand.

On the other hand, the stronger adsorption energy of C atoms with Co active phase can reduce the catalytic activity [54]; as a result, FTS process should prefer to occur on the surface with lower C adsorption energy [55]. Since C atoms adsorption ability on Co (10-10)-A surface is much weaker than that on Co(10-11) surface, Co(10-10)-A surface can prefer to catalyze FTS reaction. It is noted that for Co(10-10)-A surface, the spacing between adjacent layers is alternately short or long, which are denoted as Co(10-10)-A and Co(10-10)-B surfaces, respectively, however, the full dynamic analyses demonstrated that the equilibrium surface structure is exclusively terminated with the short interlayer spacing outermost Co(10-10)-A, which is unreconstructed [56,57].

Thus, in this study, the detailed mechanism about the C—C chain growth in FTS process will be carried out on Co(10-10)-A surface. For Co(10-10)-A surface, a six-layers $p(3 \times 2)$ surface model is employed with a 15 Å vacuum. During the calculations, the bottom two layers are fixed at its bulk positions, whereas the top four layers and all adsorbed species are relaxed, as shown in Fig. 1, four adsorption sites exist: Top, Bridge, Hcp and 4-Fold hollow sites.

3. Results and discussion

The adsorption of all possible species involved in syngas conversion over four adsorption sites of Co(10-10) have been examined, the details are presented in Part 3 of Supplementary material. Only the adsorption energies with zero-point vibrational energy correction and the key structural parameters are listed in Table 1, the most stable adsorption configurations are displayed in Fig. 2.

Since F-T synthesis is operated at the temperature ranges of 473–623 K on Co surface [8,52,53], the preferred pathway of chain growth is confirmed by the overall activation energy and the activation energy of rate-determining step together with the corresponding rate constant k at 500 K. For all elementary reactions, the activation and reaction energies with zero-point vibrational energy correction, the reaction rate constants at 500 K, and the only one imaginary frequency of the transition state on Co(10-10) surface have been listed in Table 2. The potential energy profile of these reactions with the structures of initial states (ISs), transition states (TSs) and final states (FSs) are presented in Figs. 3–13, respectively. The detailed descriptions of the calculated equations and elementary reactions are presented in Parts 4 and 5 of Supplementary material.

3.1. CO initial activation to form CH_x species

In FTS reactions, CO initial activation is the key step to determine the favored CH_x monomer, for example, DFT studies on Co (0 0 0 1) surface [58] support a hydroxyl-assisted CO activation to CH monomer, followed by the chain growth via partially hydroxyl-assisted CO insertion into HC-like RC species, R represents H or linear alkyl. Moreover, Liu et al. [59] found that COH, CHOH and CHO formation with OH-assisted route is kinetically more preferred than CHO formation with H-assisted route on Co (0 0 0 1) surface; however, both routes coincide at the same point with CHO intermediate to form CH_3OH.

For Co(10-10), our DFT studies [60] suggest that CO dissociation with H-assisted pathway leads to the formation of CH_x species. As shown in Fig. 3, the pathway of CO + H → CHO → CH + O leads to CH formation; the pathway of CO + H → CHO + H → CH_2O → CH_2 + O is responsible for CH_2 formation. CH_3 is formed by the pathway of CO + H → CHO + H → CH_2O + H → CH_3O → CH_3 + O. However, CHO prefers to be hydrogenated to CH_2O instead of being dissociated into CH and O; moreover, CH_2O dissociation into CH_2 and O is more favorable than its hydrogenation to CH_3O, suggesting that CH_2 formation is the most favorable in syngas conversion on Co (10-10). Thus, CH_2 species is the most favored monomer to join in the carbon chain growth.

3.2. The initial C–C chain formation

In general, CO, H and CH_x(x = 1–3) species are the key surface species in FTS reactions, CO is the most abundant carbon source. *In situ* spectroscopic experiments [61] confirmed CHO as the key intermediate in CO methanation on supported Ru catalysts. However, over Co(10-10) surface, our results show that CO hydrogenation to CHO at a relatively low coverage has an activation energy of 119.3 kJ mol^{-1} with a strong reaction energy of 99.2 kJ mol^{-1}, suggesting that CHO is not thermodynamically stable, which may limits CHO interactions with CH_x [29,62]. Thus, CHO intermediate is only considered as a comparison with carbide mechanism in this study. In addition, our behind results confirm that the C—C chain growth on Co(10-10) surface dominantly goes through carbide mechanism instead of CHO insertion mechanism.

Nowadays, researchers mainly focus on that what kind of CH_x will participate in the C—C chain growth, such as on the flat Co (0 0 0 1) surface, CHO insertion into CH_2 is the most facile reactions for chain growth [23], while CH self-coupling is also the most favored reactions for initial C—C chain formation [16]. Cheng et al. [63] suggest that CH_3 is the main CH_x monomer to react with CO for chain formation. Ge et al. [14] conducted CH_2 + CH coupling on the flat Co(0 0 0 1) since CH and CH_2 are regarded as the most favorable species. In this study, the C—C chain growth mechanism is extended to CH_x(x = 1–3) species, including CH_x(x = 1–3)

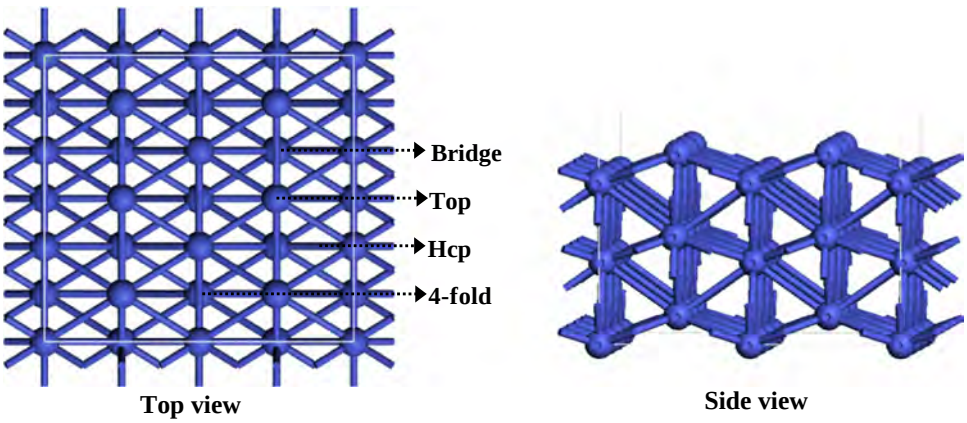

Fig. 1. The surface morphology and the corresponding adsorption sites of Co(10-10)-A surface.

Table 1
Adsorption energies (E_{ads}) and the corresponding key structural parameters of the stable configurations for the adsorbed species involving in syngas conversion on Co(10-10) surface.

Species	E_{ads} (kJ·mol^{-1})	Adsorption/configuration	D_{Co-X} (Å)	Bonding details	
				Bond	Length (Å)
CH	629.9	4 fold: via C	1.90/2.04	C—H	1.10
CH_2	375.9	hcp: via C	1.96/1.96/1.99	C—H	1.10
CH_3	185.2	bridge: via C	2.10/2.10	C—H	1.11
CH_4	3.9	away from the surface	–	C—H	1.10
H	262.3	hcp: via H	1.73/1.73/1.77	–	–
CO	168.1	hcp: via C	1.95/1.95/1.96	C—O	1.20
COH	404.3	4-fold: via C	1.88/2.09	C—O/O—H	1.37/0.98
CHO	220.1	hcp: C-bridge, O-bridge	1.91/1.98, 1.95/2.12	C—O/C—H	1.34/1.10
CH_2O	98.0	hcp: O-hcp	2.06/2.06/2.10	C—O/C—H	1.43/1.11
CH_3O	284.1	bridge: through O	1.89/1.89	C—O/C—H	1.42/1.11
CH_3OH	45.9	top: via O	2.15	C—O/C—H/O—H	1.45/1.10/0.98
C_2H_2	210.3	4 fold: α-C-4-fold, β-C-4fold	2.23/2.24, 2.23/2.24	C—C	1.41
CH_2CH	282.0	hcp: α-C-hcp, β-C-hcp	1.94/1.97/2.07, 2.11/2.26/2.45	C—C	1.47
CH_3CH	343.7	hcp: via α-C	1.97/1.98/2.01	C—C	1.52
C_2H_4	92.3	bridge: α-C-bridge, β-C-top	2.11/2.34,2.02	C—C	1.43
CH_3CH_2	161.0	bridge: via α-C	2.11/2.11	C—C	1.53
C_2H_6	10.2	away from the surface	–	C—C	1.53
CHCO	330.6	α-C-hcp, β-C-4 fold	1.99/2.00/2.01, 2.03/2.12	C—C/C—O/C—H	1.43/1.27/1.10
CH_2CO	118.7	bridge: α-C-top, β-C-bridge	1.81, 2.07/2.12	C—C /C—O	1.51/1.21
CH_3CO	236.4	bridge: α-C-top, O-top	1.85/1.98	C—C/C—O/	1.51/1.27
CHCHO	421.4	β-C-4 fold, O-bridge	1.97/2.01, 2.01/2.02	C—C/C—O	1.42/1.35
CH_2CHO	220.8	bridge: β-C-top, O-top	2.10, 1.87	C—C/C—O	1.41/1.33
CH_3CHO	60.6	bridge: α-C-bridge, O-top	2.32/2.18, 1.87	C—C/C—O	1.50/1.33
CH_3CH_2O	264.3	bridge: via O	1.93/1.93	C—C/C—O	1.52/1.45
CHCHOH	287.4	hcp: via β-C	1.96/2.02/2.03	C—C/C—O	1.42/1.37
CH_2CHOH	83.8	bridge: α-C-top, O-top	2.20/2.08	C—C/C—O	1.40/1.42
CH_3CHOH	159.3	bridge: α-C-top, O-top	2.00/2.10	C—C/C—O	1.51/1.47
C_2H_5OH	48.0	top: via O	2.15	C—C/C—O	1.51/1.46
CH_3CH_2CH	345.6	hcp: via α-C	1.92/1.96/2.07	C—C—C	1.53/1.52
$CH_3CH_2CH_2$	165.9	bridge: via α-C	2.06/2.12	C—C—C	1.53/1.53
C_3H_8	9.1	away from the surface		C—C—C	1.53/1.53
CH_3CH_2CHO	77.9	bridge: α-C-top, O-bridge	2.03, 1.95/2.05	C—C—C/C—O	1.54/1.51, 1.34
$CH_3CH_2CH_2O$	265.9	bridge: via O	1.92/1.92	C—C—C/C—O	1.53/1.52, 1.43
CH_3CH_2CHOH	141.7	bridge: α-C-top, O-top	1.99, 2.15	C—C—C/C—O	1.53/1.50, 1.44
$CH_3CH_2CH_2OH$	48.6	top: via O	2.15	C—C—C/C—O	1.53/1.51, 1.46
$CH_3CH_2CH_2CH_2$	166.8	bridge: via α-C	2.09/2.13	C—C—C—C	1.53/1.54/1.65
$CH_3CH_2CH_2CHO$	91.3	bridge: α-C-top, O-bridge	2.03, 1.99/2.00	C—C—C—C/C—O	1.53/1.53/1.51, 1.34

self-coupling and CO/CHO insertion into CH_x(x = 1–3) on Co(10-10) surface.

3.2.1. CH related reactions

As shown in Fig. 4, among all reactions related to CH species, CH hydrogenation to CH_2 and CHO insertion into CH to CHCHO are two parallel and favorable reactions in kinetics, namely, CH_2 and CHCHO are the dominant products. Meanwhile, CH dissociation to C and H is difficult due to the high activation energy, suggesting that Co(10-10) surface exhibits low catalytic activity toward CH dissociation in kinetics, which will inhibit C deposition on the catalyst surface. In addition, CH coupling with other CH_x or CO insertion into CH is also difficult due to higher activation energies.

Thus, starting from CH species, CHO insertion into CH to CHCHO is the most favorable, which contributes to the initial C—C chain formation; CH is also easily hydrogenated to CH_2.

3.2.2. CH_2 related reactions

As shown in Fig. 5, among all reactions related to CH_2, CH_2 self-coupling to C_2H_4 and CHO insertion into CH_2 to CH_2CHO are two parallel pathways for initial C—C chain growth in kinetics. Then, CH_2 hydrogenation to CH_3 also occur with an activation energy of 44.4 kJ mol^{-1}.

3.2.3. CH_3 related reactions

From Fig. 6, among all reactions related to CH_3 species, CHO insertion into CH_3 to CH_3CHO is favorable kinetically. Meanwhile, CH_3 hydrogenation to CH_4 also occur with an activation energy of 82.4 kJ mol^{-1}. Thus, starting from CH_3 species, CHO insertion into CH_3 to CH_3CHO is the preferable pathway for the initial C—C chain formation related to CH_3 in kinetics.

3.2.4. Brief summary about the initial C–C chain formation

As mentioned above, when CH, CH_2 and CH_3 species co-exist over Co surface, CHO insertion into CH, CH_2 self-coupling, CHO insertion into CH_2, and CHO insertion into CH_3 are the four favorable pathways for the initial C—C chain growth in kinetics, which correspond to CH, CH_2 and CH_3 species, respectively, suggesting that the initial C—C chain formation on Co(10-10) can be realized *via* both carbide mechanism and CHO insertion mechanism; however, CHO insertion into CH and CH_2 to CHCHO and CH_2CHO are more preferred to realize the initial C—C chain formation on Co (0 0 0 1) [27]. Thus, the initial C—C chain formation is sensitive to the crystal facet of Hcp Co.

Among four optimal reactions of initial C—C chain formation, CH_2 self-coupling (31.4 kJ·mol^{-1}) and CHO insertion into CH_2 (34.9 kJ·mol^{-1}) possess relatively low activation energies, and both are more preferable than other reactions in kinetics, which accord with previous results [16] that CH_2 self-coupling is the most favorable in all reactions of CH_x + CH_y coupling on the stepped Co(0 0 0 1) surface, respectively. Moreover, CHO insertion into CH_2 is the most accessible one among all reactions related to CO and CHO insertion into CH_x on the flat Co(0 0 0 1) surface [23]. Further, CH_2 is the most favored monomer among all CH_x species on Rh surface, and CO insertion into CH_2 is deduced to be the precursor for

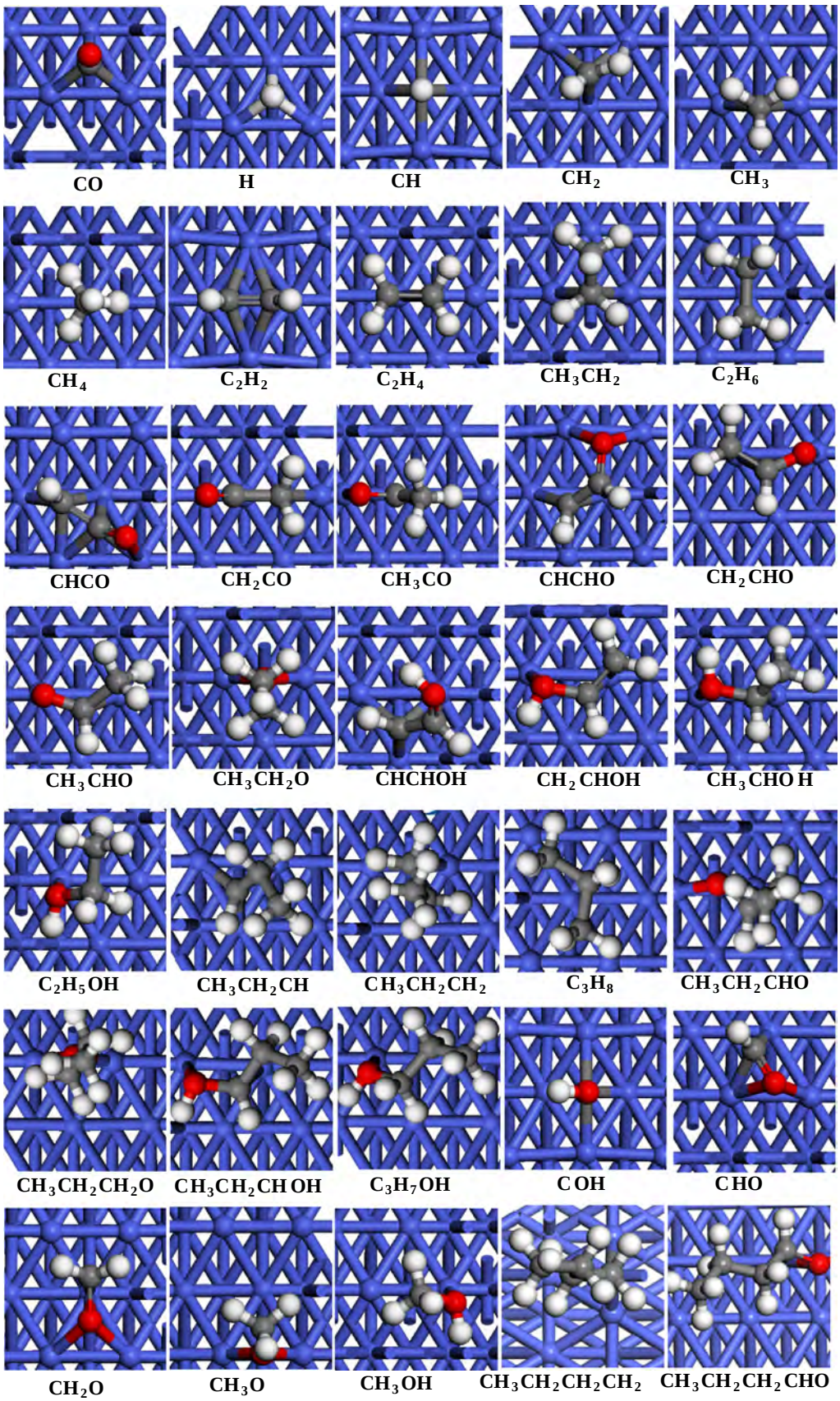

Fig. 2. The most stable adsorption configurations of all possible species involved in the C—C chain growth on Co(10-10) surface. Co, C, H and O atoms are shown in the blue, grey, white and red balls, respectively.

Table 2
All possible elementary reactions and the corresponding activation energy (E_a, kJ·mol^{-1}) and reaction energies (ΔE, kJ·mol^{-1}), the reaction rate constant (k, s^{-1}) at 500 K, as well as the only one imaginary frequency of transition state (ν, cm^{-1}) involving in syngas conversion on Co(10-10) surface.

	Reactions	TS	ν	E_a	ΔE	k
R1-1	CO → C+O	TS1-1	398*i*	187.5	60.6	3.24×10^{-8}
R1-2	C + H → CH	TS1-2	921*i*	65.6	−28.9	1.45×10^{6}
R1-3	CO + H → COH	TS1-3	1513*i*	158.8	95.6	9.01×10^{-5}
R1-4	CO + H → CHO	TS1-4	625*i*	119.3	99.2	9.80×10^{-1}
R1-5	CHO → CH + O	TS1-5	449*i*	45.2	−84.0	1.04×10^{8}
R1-6	CHO + H → CH_2O	TS1-6	801*i*	33.1	4.8	1.58×10^{9}
R1-7	CH_2O → CH_2 + O	TS1-7	435*i*	27.2	−27.3	6.39×10^{9}
R1-8	CH_2O + H → CH_3O	TS1-8	375*i*	49.6	−38.5	5.17×10^{7}
R1-9	CH_3O → CH_3 + O	TS1-9	585*i*	132.2	−39.1	1.70×10^{-1}
R1-10	CH_3O + H → CH_3OH	TS1-10	1237*i*	124.3	51.9	2.80×10^{-4}
R2-1	CH → C + H	TS2-1	921*i*	94.5	28.9	5.16×10^{4}
R2-2	CH + H → CH_2	TS2-2	947*i*	53.7	22.9	2.41×10^{7}
R2-3	CH + CH → C_2H_2	TS2-3	432*i*	88.3	17.5	2.90×10^{3}
R2-4	CH + CO → CHCO	TS2-4	342*i*	83.2	57.0	5.53×10^{3}
R2-5	CH + CHO → CHCHO	TS2-5	179*i*	48.5	20.0	3.99×10^{7}
R3-1	CH_2 + H → CH_3	TS3-1	887*i*	44.4	−30.9	8.62×10^{5}
R3-2	CH_2 + CH_2 → C_2H_4	TS3-2	382*i*	31.4	−70.1	3.38×10^{9}
R3-3	CH_2 + CO → CH_2CO	TS3-3	343*i*	58.3	43.9	2.61×10^{7}
R3-4	CH_2 + CHO → CH_2CHO	TS3-4	306*i*	34.9	−61.4	3.18×10^{9}
R4-1	CH_3 + H → CH_4	TS4-1	783*i*	82.4	12.7	7.67×10^{4}
R4-2	CH_3 + CH_3 → C_2H_6	TS4-2	575*i*	276.7	7.2	2.92×10^{-16}
R4-3	CH_3 + CO → CH_3CO	TS4-3	423*i*	112.9	53.2	5.72×10^{1}
R4-4	CH_3 + CHO → CH_3CHO	TS4-4	406*i*	69.0	−14.5	5.58×10^{5}
R4-5	CH_3 + CH_2 → CH_3CH_2	TS4-5	433*i*	77.7	−30.1	1.06×10^{5}
R5-1	CHCHO → C_2H_2 + O	TS5-1	483*i*	72.9	−40.0	9.46×10^{5}
R5-2	CHCHO + H → CHCHOH	TS5-2	1312*i*	138.3	48.8	8.25×10^{-2}
R5-3	CHCHO + H → CH_2CHO	TS5-3	914*i*	52.3	8.7	1.56×10^{8}
R5-4	CH_2CHO → CH_2CH + O	TS5-4	535*i*	134.8	−31.0	1.36×10^{-1}
R5-5	CH_2CHO + H → CH_2CHOH	TS5-5	1246*i*	81.6	44.8	5.25×10^{3}
R5-6	CH_2CHO + H → CH_3CHO	TS5-6	823*i*	27.7	20.0	1.18×10^{10}
R5-7	CH_3CHO → CH_3CH + O	TS5-7	527*i*	70.2	−40.1	3.02×10^{5}
R5-8	CH_3CHO + H → CH_3CHOH	TS5-8	1049*i*	112.1	29.2	6.69×10^{1}
R5-9	CH_3CHO + H → CH_3CH_2O	TS5-9	885*i*	21.6	−30.8	3.31×10^{10}
R5-10	CH_3CH_2O → CH_3CH_2 + O	TS5-10	520*i*	114.1	−12.1	1.98×10^{1}
R5-11	CH_3CH_2O + H → CH_3CH_2OH	TS5-11	1205*i*	112.2	58.7	3.04×10^{2}
R5-12	C_2H_4 + H → CH_3CH_2	TS5-12	792*i*	8.1	−7.2	2.88×10^{11}
R6-1	CH_3CH_2 + H → C_2H_6	TS6-1	809*i*	71.9	4.6	3.87×10^{5}
R6-2	CH_3CH_2 + CH_2 → $CH_3CH_2CH_2$	TS6-2	333*i*	72.5	−41.8	1.81×10^{5}
R6-3	CH_3CH_2 + CHO → CH_3CH_2CHO	TS6-3	355*i*	61.1	−45.2	2.11×10^{6}
R7-1	CH_3CH_2CHO → CH_3CH_2CH + O	TS7-1	495*i*	81.1	−25.5	2.74×10^{4}
R7-2	CH_3CH_2CHO + H → CH_3CH_2CHOH	TS7-2	1301*i*	103.3	70.3	1.59×10^{2}
R7-3	CH_3CH_2CHO + H → $CH_3CH_2CH_2O$	TS7-3	816*i*	34.9	−18.6	5.33×10^{9}
R7-4	$CH_3CH_2CH_2O$ → $CH_3CH_2CH_2$ + O	TS7-4	399*i*	131.1	−9.4	7.58×10^{-2}
R7-5	$CH_3CH_2CH_2O$ + H → $CH_3CH_2CH_2OH$	TS7-5	970*i*	116.8	58.6	3.29×10^{1}
R8-1	$CH_3CH_2CH_2$ + H → C_3H_8	TS8-1	874*i*	53.9	−13.1	7.48×10^{6}
R8-2	$CH_3CH_2CH_2$ + CH_2 → $CH_3CH_2CH_2CH_2$	TS8-2	260*i*	41.0	−65.0	5.24×10^{8}
R8-3	$CH_3CH_2CH_2$ + CHO → $CH_3CH_2CH_2CHO$	TS8-3	250*i*	52.7	−61.7	2.20×10^{6}

C_2 oxygenates formation from syngas [64]. Thus, our results further confirm that CH_2 species is the most favored monomer among all CH_x species on Co(10-10) surface, which is dominantly responsible for the initial C—C chain formation. In addition, since CH_2 hydrogenation to CH_3 and CH_2 dissociation into CH are easy to occur with the small activation energies of 44.4 and 30.8 kJ·mol^{-1}, thus, a small quantity of CH and CH_3 species formed by CH_2 dissociation and hydrogenation can exist.

Fig. 7 presents the potential energy profile for the optimal pathways of CH_3OH and CH_4 formation with respect to CO + H species on Co(10-10) surface, the results show that Co(10-10) surface exhibits a good catalytic performance towards CH_2 formation, and inhibit CH_3OH formation due to the higher activation energy. However, taking the reactions related to CH_x(x = 1–3) species into consideration, CH_4 can be formed by the partial CH_x(x = 1–3) hydrogenation. The relative selectivity of CH_3OH and CH_4 will be examined using microkinetic modeling in Section 3.6.

On the other hand, although a small quantity of CH and CH_3 species can exist, CH dissociation is more difficult than its hydrogenation, suggesting that Co(10-10) surface can inhibit C formation, as a result, the reactions related to C species, C + OH → COH, C + CO → CCO, C + C → CC, C + CH → CCH, C + CH_2 → CCH_2 and C + CH_3 → CCH_3 are not considered. Secondly, taking the subsequent reactions from CH, CH_2 and CH_3 species, it is possible to have the self-coupling of CH_x species at high coverage, but it is not possible to have cross-coupling, and this is because that only one type of surface intermediate is (or most) preferred; thus, the CH_x cross-coupling reactions, CH + CH_2 → $CHCH_2$, CH + CH_3 → $CHCH_3$ and CH_2 + CH_3 → CH_2CH_3, are not examined. Thirdly, since the most favored CH_2 monomer is formed by the pathway of CO + H → CHO + H → CH_2O → CH_2 + O, the O and OH species formed by O hydrogenation under the FTS hydrogen-rich conditions. CH_x(x = 1–3) species may interact with the O and OH species to form CH_xO and CH_xOH species, however, this study show that CH_xO dissociation into CH_x(x = 1–3) and O species is more easier than its reverse reactions; Our previous studies [60] also show that CH_xOH dissociation into CH_x and OH species is more favorable than its reverse reactions; hence, the O and OH species dominantly prefers to be hydrogenated to H_2O instead of being interacted with CH_x(x = 1–3) species to CH_xO and CH_xOH species, the reactions of CH_x(x = 1–3) + OH → CH_xOH(x = 1–3) and CH_x(x = 1–3) + O → CH_xO(x = 1–3) are not discussed in this study.

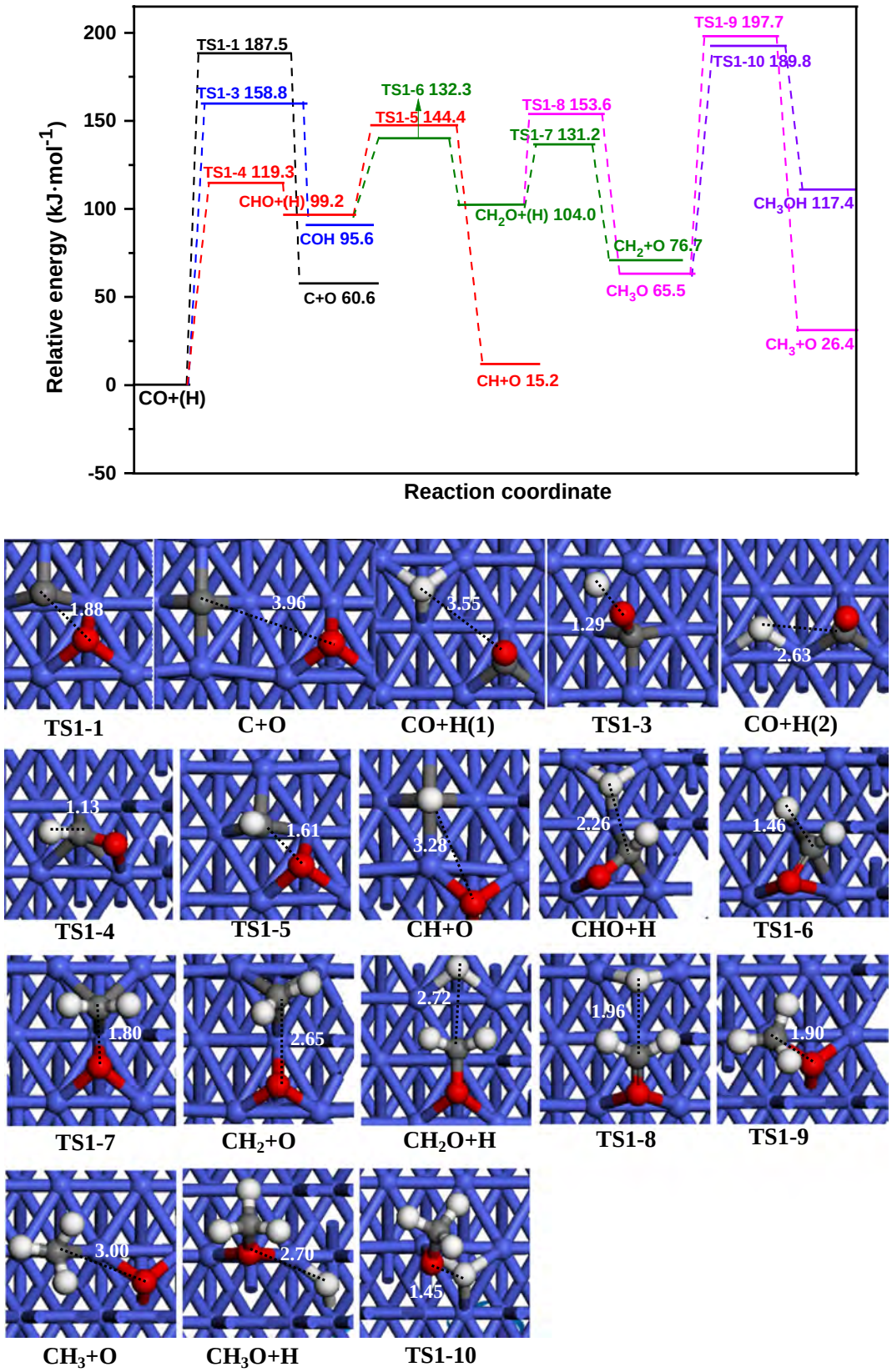

Fig. 3. The potential energy profiles of CH_x(x = 1–3) and CH_3OH formation with respect to CO + H species on Co(10-10) surface together with the structures of transition states (TSs) and co-adsorbed species. Other structures are shown in Fig. 2. Bond lengths are in Å.

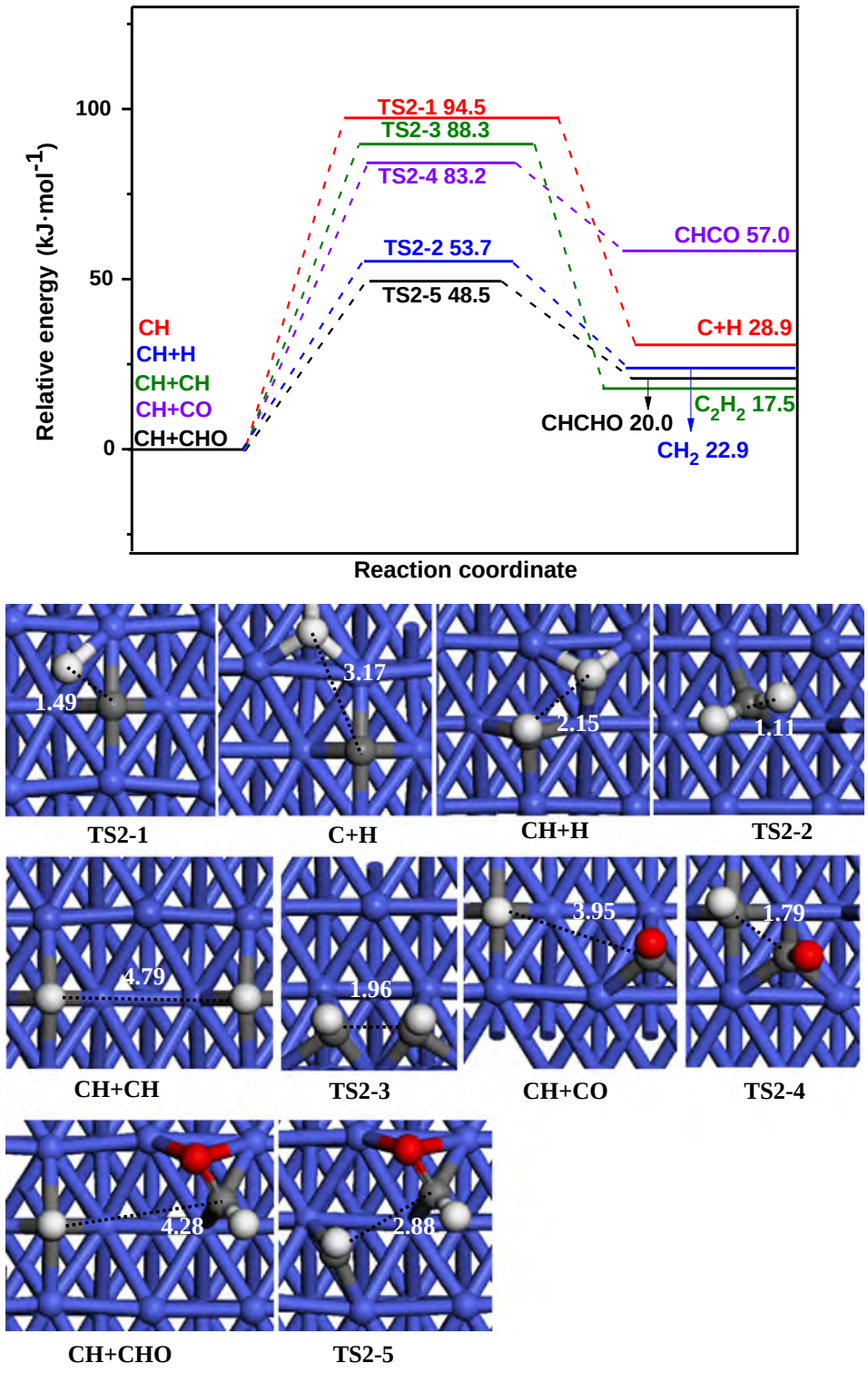

Fig. 4. The potential energy profile of the reactions related to CH species together with the structures of transition states (TSs) and co-adsorbed species on Co(10-10) surface. Other structures are shown in Fig. 2. Bond lengths are in Å.

3.3. C_2H_x intermediate formation

For C_2H_x formation, based on above analysis about the initial C—C chain formation, CH_2 self-coupling to C_2H_4 is the most preferable reactions related to CH_x species in kinetics. It should be noted that on Co(10-10) surface, CHO insertion is more superior to CO insertion into CH_x for the initial — chain growth in kinetics, this result agrees with previous DFT results [23], this superiority may attribute to the smaller HOMO–LUMO gap of CHO compared to CO, which promotes the charge transfer and hybridization with the surface. More importantly, CO insertion into CH_x to CH_xCO on Co(0 0 0 1) surface indicated that the C—O bond of CH_xCO can be hardly broken, while the C—O bond cleavage of CH_xCHO can be easily realized [19]. Moreover, CH_xCO always prefer to be hydro-

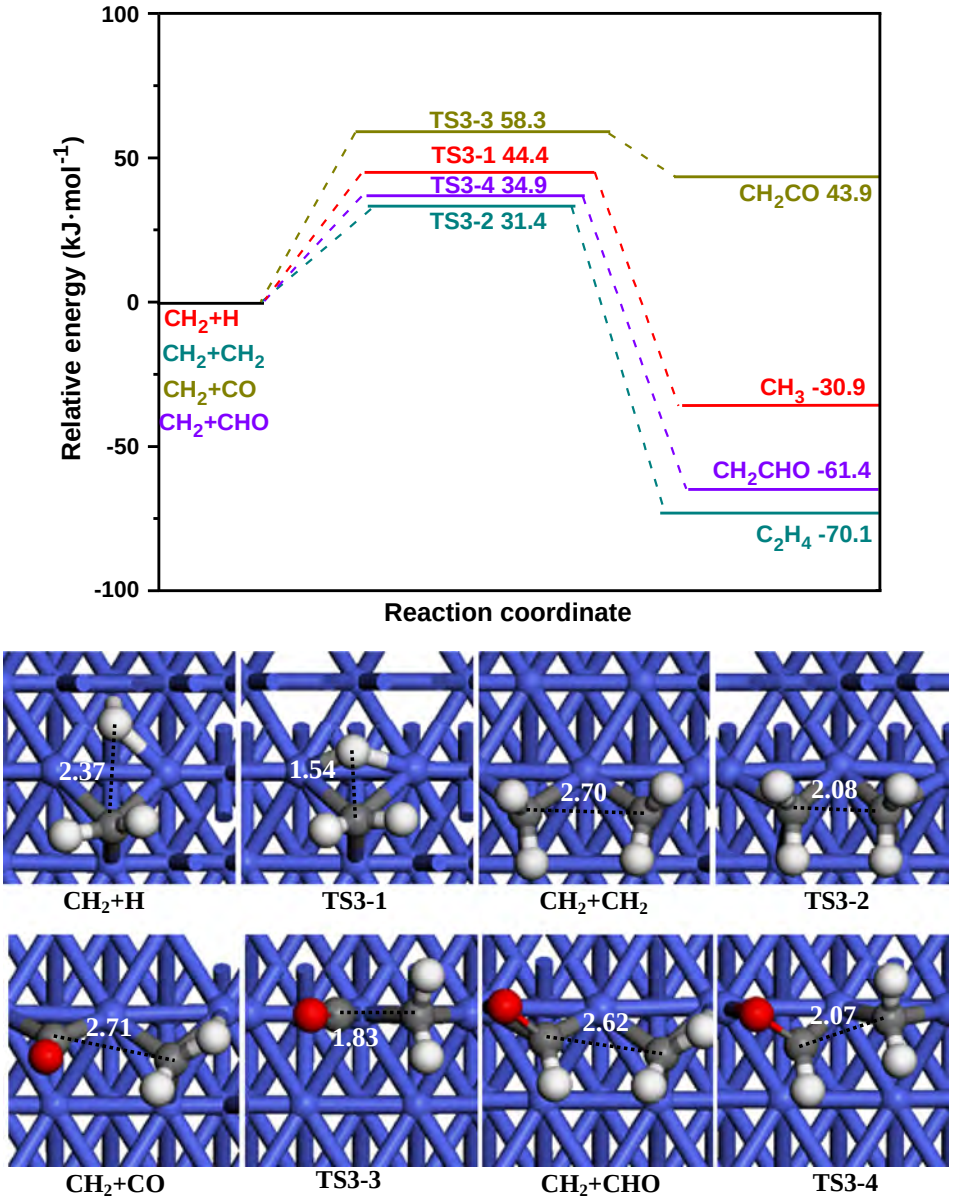

Fig. 5. The potential energy profile of the reactions related to CH_2 species together with the structures of transition states (TSs) and co-adsorbed species on Co(10-10) surface. Other structures are shown in Fig. 2. Bond lengths are in Å.

genated to CH_xCHO [22,65], as a result, the C—O bond of CH_xCO has not been considered in this study. Notably, the formed CH_xCO *via* CO insertion on Co(0 0 0 1) surface [63] and the formed CH_xCHO *via* CHO insertion on Cu-doped Co(0 0 0 1) surface [26] can be successively hydrogenated, which is responsible for C_2 oxygenate formation. Thus, starting from CH_xCHO on Co(10-10) surface, its C—O bond scission is examined to probe into whether CHO insertion mechanism and/or carbide mechanism is dominantly responsible for C_2H_x formation.

Starting from CH_xCHO, its C—O bond scission will form CH_xCH, alternatively, it can be also hydrogenated to $CH_{x+1}CHO$, CH_xCH_2O or CH_xCHOH, respectively. As shown in Fig. 8 (see details in the Part 4 of Supplementary material), CH_xCHO prefers to be hydrogenated to $CH_{x+1}CHO$ in kinetics, followed by the successive hydrogenation to CH_3CH_2O rather than being dissociated into CH_xCH and their desorption. However, the C—C chain growth on Co(0 0 0 1) surface [27] suggests that CH_3CHO prefers to be dissociated into CH_3CH intermediate rather than being hydrogenated to CH_3CH_2O, namely, the C—O bond scission of CH_3CHO to form CH_3CH on Co(0 0 0 1) surface is in favor of the C—C chain growth *via* CHO insertion mechanism.

Fig. 9 presents the potential energy profile of the most favorable pathways for C_2H_x formation, suggesting that CHCHO prefers to be hydrogenated to CH_2CHO in kinetics; meanwhile, CHO insertion into CH_2 also contributes to CH_2CHO, followed by the successive hydrogenation to CH_3CH_2O via CH_3CHO intermediate. Further, CH_3CH_2O dissociation into CH_3CH_2 has a high activation energy of 114.1 kJ mol^{-1} and the rate constant of $1.98 \times 10^1\ s^{-1}$, which is also the rate-limiting step for CH_3CH_2 formation *via* CHO insertion mechanism. However, among above these reactions of C_2H_x formation, CH_2 self-coupling to C_2H_4 is the most favorable with the lowest activation energy of 31.4 kJ mol^{-1} and the rate constant of $3.38 \times 10^9\ s^{-1}$; subsequently, as presented in **R5-12**, C_2H_4 prefers to be hydrogenated to CH_3CH_2 with only an activation energy of 8.1 kJ mol^{-1} and a rate constant of $2.88 \times 10^{11}\ s^{-1}$ rather than its desorption (92.3 kJ mol^{-1}).

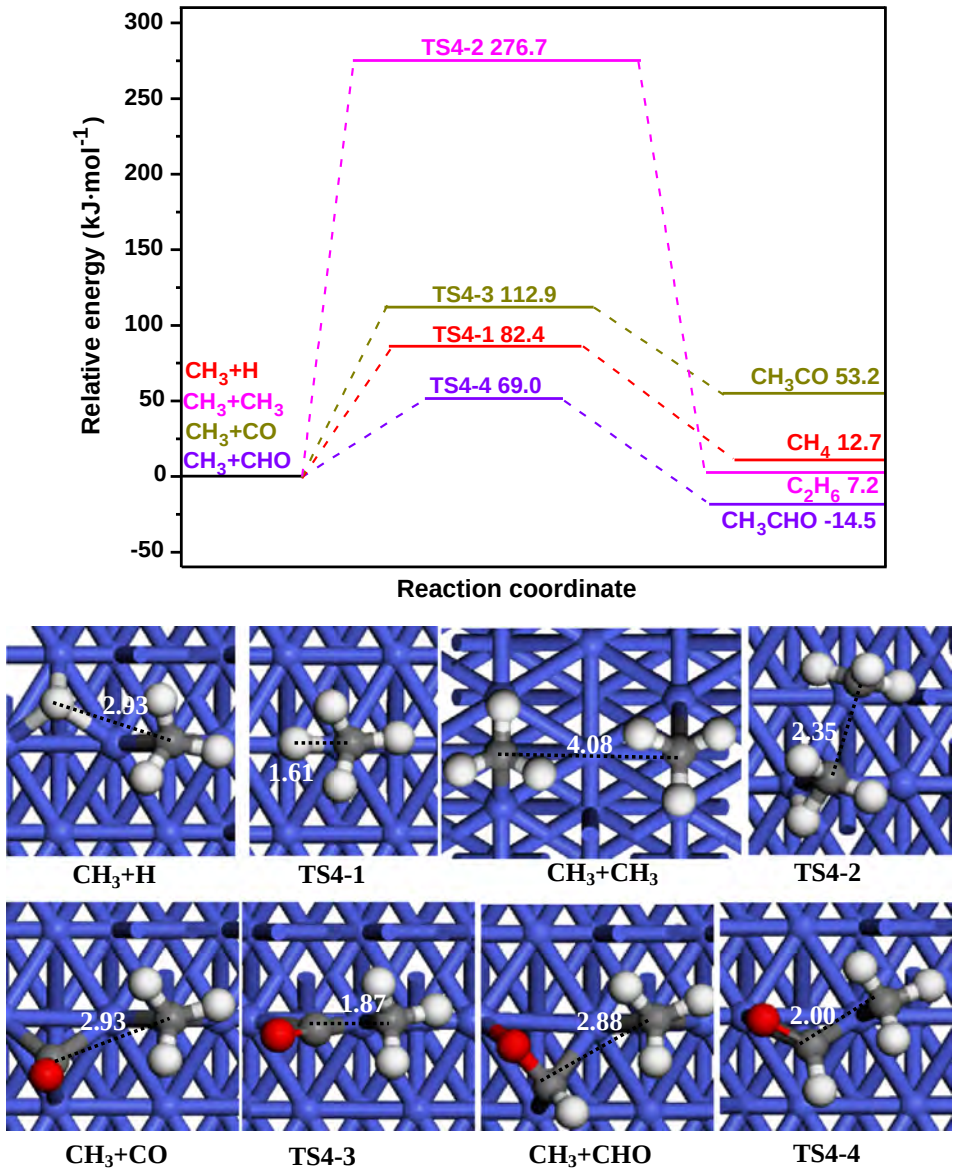

Fig. 6. The potential energy profile of the reactions related to CH_3 species together with the structures of transition states (TSs) and co-adsorbed species on Co(10-10) surface. Other structures are shown in Fig. 2. Bond lengths are in Å.

Thus, CH_3CH_2 intermediate is the most favorable C_2H_x species in kinetics, which dominantly comes from CH_2 self-coupling to C_2H_4, followed by its hydrogenation rather than that *via* CHO insertion mechanism. Namely, the most favorable C_2H_x species dominantly comes from carbide mechanism rather than CHO insertion mechanism.

3.4. C_3H_x intermediate formation

As mentioned above, CH_3CH_2 intermediate is the most abundant C_2H_x species, in order to investigate the mechanism of the further C—C chain growth, the reactions related to CH_3CH_2 species, including hydrogenation, self-coupling with the most favored CH_2 monomer via carbide mechanism, and CHO insertion via CHO insertion mechanism are further considered.

As shown in Fig. 10 (see details in the Supplementary material), CHO insertion into CH_3CH_2 has the lowest activation energy of 61.1 kJ mol^{-1} in kinetics with the rate constant of $2.11 \times 10^6\ s^{-1}$. Moreover, $CH_3CH_2 + CH_2$ coupling to $CH_3CH_2CH_2$ and CH_3CH_2 hydrogenation to C_2H_6 have the similar activation energies of 72.5 and 71.9 kJ mol^{-1} with the corresponding rate constants of 1.81×10^5 and $3.87 \times 10^5\ s^{-1}$, respectively. Thus, for the C—C chain growth from C_2 to C_3 species, $CH_3CH_2 + CH_2$ coupling to CH_3CH_2-CH_2 that belongs to carbide mechanism is also compatible with CHO insertion into CH_3CH_2 in kinetics.

Starting from CH_3CH_2CHO (see Fig. S1), it prefers to hydrogenate to $CH_3CH_2CH_2O$ instead of being dissociated into CH_3CH_2CH *via* the scission of C—O bond and being hydrogenated to CH_3CH_2CHOH; then, $CH_3CH_2CH_2O$ dissociates or hydrogenates into $CH_3CH_2CH_2$ or $CH_3CH_2CH_2OH$, respectively.

As shown in Fig. 11, CH3CH2 coupling with CH_2 to $CH_3CH_2CH_2$ is slightly unfavorable compared to CHO insertion into CH_3CH_2 to CH_3CH_2CHO, followed by hydrogenation to $CH_3CH_2CH_2O$. However, $CH_3CH_2CH_2O$ dissociation into $CH_3CH_2CH_2 + O$ has a significantly high activation energy (131.1 kJ mol^{-1}), which is also the rate limiting-step of CHO insertion mechanism for $CH_3CH_2CH_2$ formation. Thus, for C_3H_x formation, $CH_3CH_2CH_2$ is the most favored C_3 species, which is dominantly formed via carbide mechanism of $CH_3CH_2 + CH_2$ coupling rather than that via CHO insertion mechanism. This result is similar to CH_3CH_2 formation via carbide

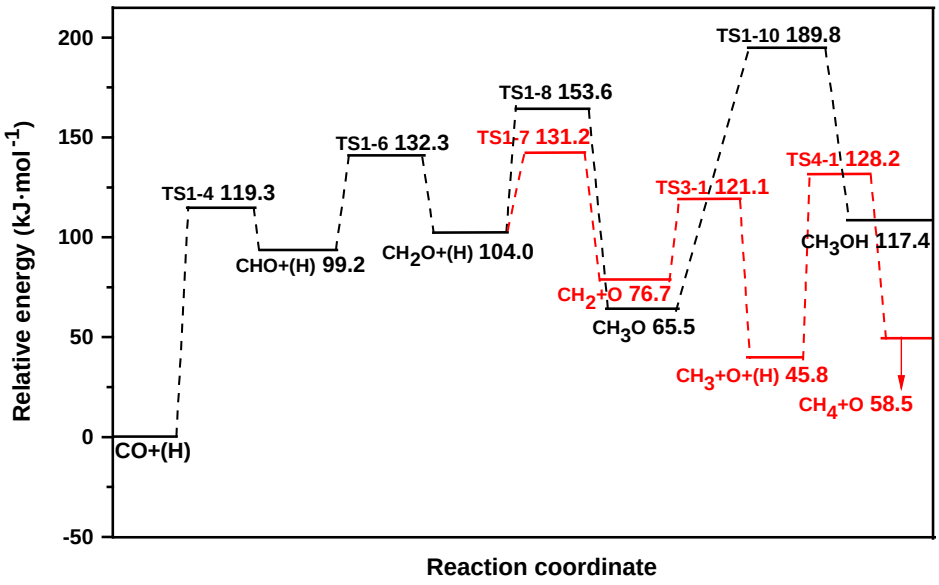

Fig. 7. The potential energy profiles of CH_3OH and CH_4 formation with respect to CO+H species on Co(10-10) surface.

mechanism of CH_2 self-coupling to C_2H_4, followed by its hydrogenation, as well as CH_3 coupling with CH_2.

Fig. 12 presents the potential energy profile of the optimal coupling pathways for C_2H_6 and C_3H_8 formation on Co(10-10) surface, suggesting that CH_2 self-coupling and $CH_3CH_2 + CH_2$ coupling can form C_2H_4 and $CH_3CH_2CH_2$, followed by the successive hydrogenation to realize the formation of C_2H_6 and C_3H_8 species.

3.5. C_4H_x intermediate formation

In order to further investigate the chain growth mechanism, we conduct the C—C chain growth from C_3 to C_4 species. As mentioned above, CH_3CH_2 interaction with H, CH_2 and CHO species are examined. Thus, for CH_3CH_2-like species, $CH_3CH_2CH_2$, $CH_3CH_2CH_2 + H \rightarrow CH_3CH_2CH_3$ (R8-1) and $CH_3CH_2CH_2 + CH_2 \rightarrow CH_3CH_2CH_2CH_2$ (R8-2) and $CH_3CH_2CH_2 + CHO \rightarrow CH_3CH_2CH_2CHO$ (R8-3) are considered.

As shown in Fig. 13, for CH3CH2CH2 hydrogenation, CH_3CH_2-$CH_2 + CH_2$ coupling, and CHO insertion into $CH_3CH_2CH_2$, these three reactions have lower activation energies than the corresponding reaction related to CH_3CH_2 species; moreover, CH_3CH_2-$CH_2 + CH_2$ coupling to $CH_3CH_2CH_2CH_2$ is the most favorable reaction.

Therefore, C_4H_x formation will follow the similar pathways with C_3H_x formation, and $CH_3CH_2CH_2CH_2$ intermediate is the most favored C_4H_x species in kinetics, which mainly comes from the carbide mechanism via $CH_3CH_2CH_2$ coupling with the most favored monomer CH_2.

3.6. Microkinetic modeling

By microkinetics modeling, the product distribution can be obtained based on the equilibrium constants of reactants and the kinetic parameters of reactions. More importantly, microkinetics modeling can consider the effects of reaction temperature, pressure, and the terms of coverage for all intermediate species involved in the reaction mechanism under the realistic conditions [66–69]. In this study, microkinetic modeling has been employed on Co(10-10) surface to obtain the relative selectivity of products CH_3OH (r_{CH_3OH}), CH_4 (r_{CH_4}), C_2H_5OH ($r_{C_2H_5OH}$), C_2H_6 ($r_{C_2H_6}$), C_3H_7OH ($r_{C_3H_7OH}$) C_3H_8 (r_{C_{3}H_{8}}) under typical FTS conditions (P_{CO} = 5 atm, P_{H_2} = 10 atm, and T = 500 K), as listed in Table 3. The detailed descriptions are given out in Part 6 of the Supplementary material. Fig. 14 lists all elementary steps involved in the preferred formation pathways of CH_3OH, CH_4, C_2H_5OH, C_2H_6, C_3H_7OH, and C_3H_8 with the activation and reaction energies.

On Co(10-10), on one hand, the relative selectivity of CH_4 can reach 17.72% approximately, which is higher than CH_3OH, C_2H_5OH and C_3H_7OH, the relative selectivity of total alcohols can be ignored. On the other hand, the relative selectivity of C_3H_8 can reach up to 61.65%, which is much higher than C_2H_6 with 9.56% and CH_4, this result corresponds to that Co catalyst is in favor of the longer C—C chain formation of hydrocarbons [7,8]. Namely, Co(10-10) surface exhibits a better catalytic activity and selectivity towards the C—C chain formation of hydrocarbons.

3.7. Proposed the mechanism of C—C chain growth

On the basis of the initiation and growth of C—C chain on Co(10-10), Fig. 14 presents the optimal pathway from CH_x to C_4H_x hydrocarbons.

For the initial C—C chain formation, starting from CH_x(x = 1–3) species, CHO insertion into CH, CH_2 and CH_3, as well as CH_2 coupling with CH_2 are four preferable reactions in kinetics. However, CHO is not thermodynamically stable on Co(10-10) surface, which limits its interactions with CH_x intermediates [29,62]. Thus, the initial C—C chain formation on Co(10-10) surface is mainly realized via carbide mechanism instead of CHO insertion mechanism.

For C_2H_x formation, CH_2 self-coupling to C_2H_4 is the most favorable; subsequently, C_2H_4 hydrogenation can easily form CH_3CH_2 as the dominant C_2H_x species in kinetics; thus, C_2H_x is formed *via* carbide mechanism. For C_3H_x species, starting from CH_3CH_2 intermediate, CH_3CH_2 coupling with CH_2 leads to $CH_3CH_2CH_2$ as the dominant C_3H_x species, which is also formed *via* carbide mechanism. For C_4H_x species, $CH_3CH_2CH_2$ coupling with CH_2 results in $CH_3CH_2CH_2CH_2$ intermediate as the favored C_4 species, which is mainly formed *via* carbide mechanism.

Thus, the C—C chain growth process of $C_1 \rightarrow C_2 \rightarrow C_3 \rightarrow C_4$ hydrocarbons on Co(10-10) surface show that the C—C chain growth mainly focuses on the most favored monomer CH_2 coupling with RCH_2 to form $R'CH_2$ (R represents alkyl or H, and R' equals to RCH_2); subsequently, the favored monomer CH_2 coupling with

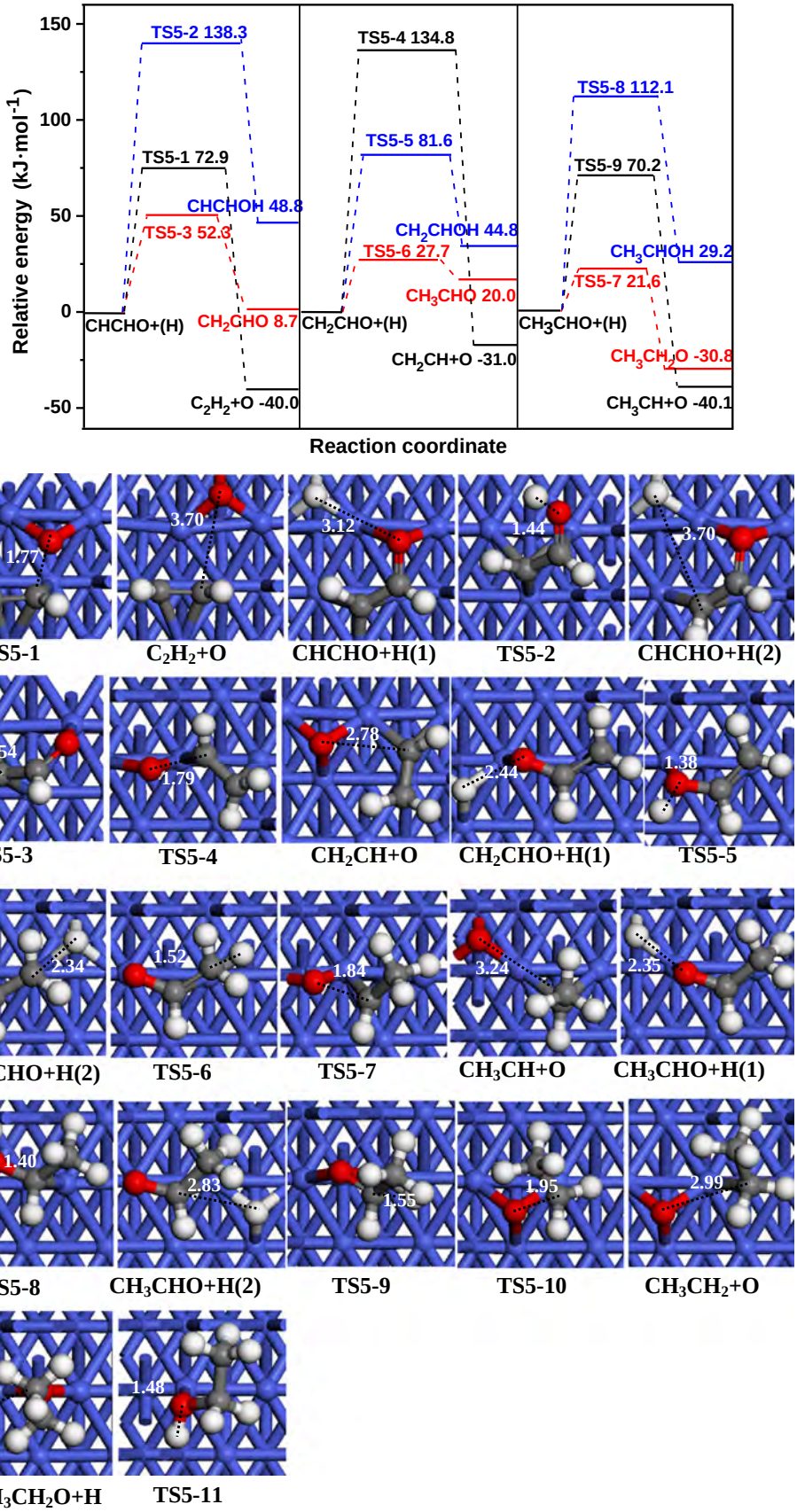

Fig. 8. The potential energy profile of the reactions related to CH_xCHO(x = 1–3) species together with the possible structures of transition states (TSs) and co-adsorbed species on Co(10-10) surface. Other structures are shown in Fig. 2. Bond lengths are in Å.

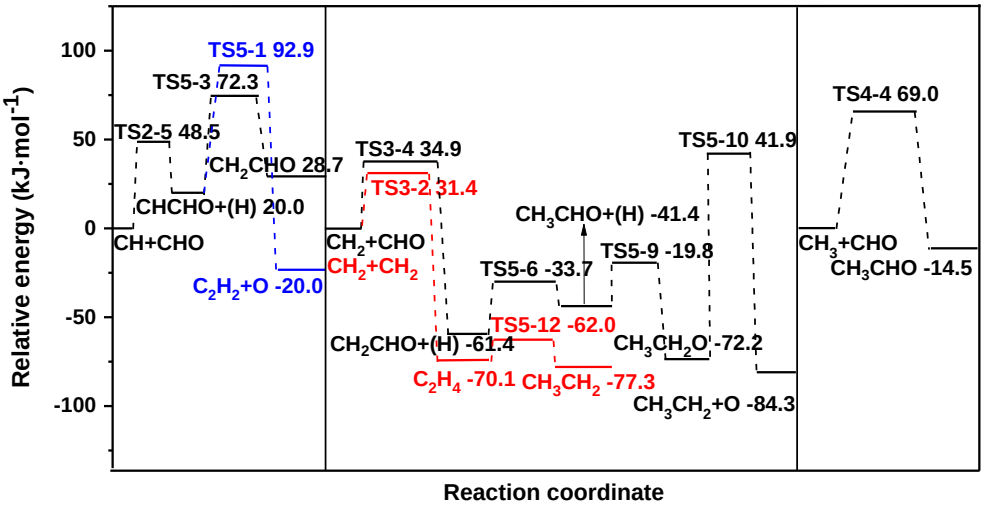

Fig. 9. The potential energy profile of the optimal coupling and CHO insertion into CH_x(x = 1–3) for C_2H_x formation on Co(10-10) surface.

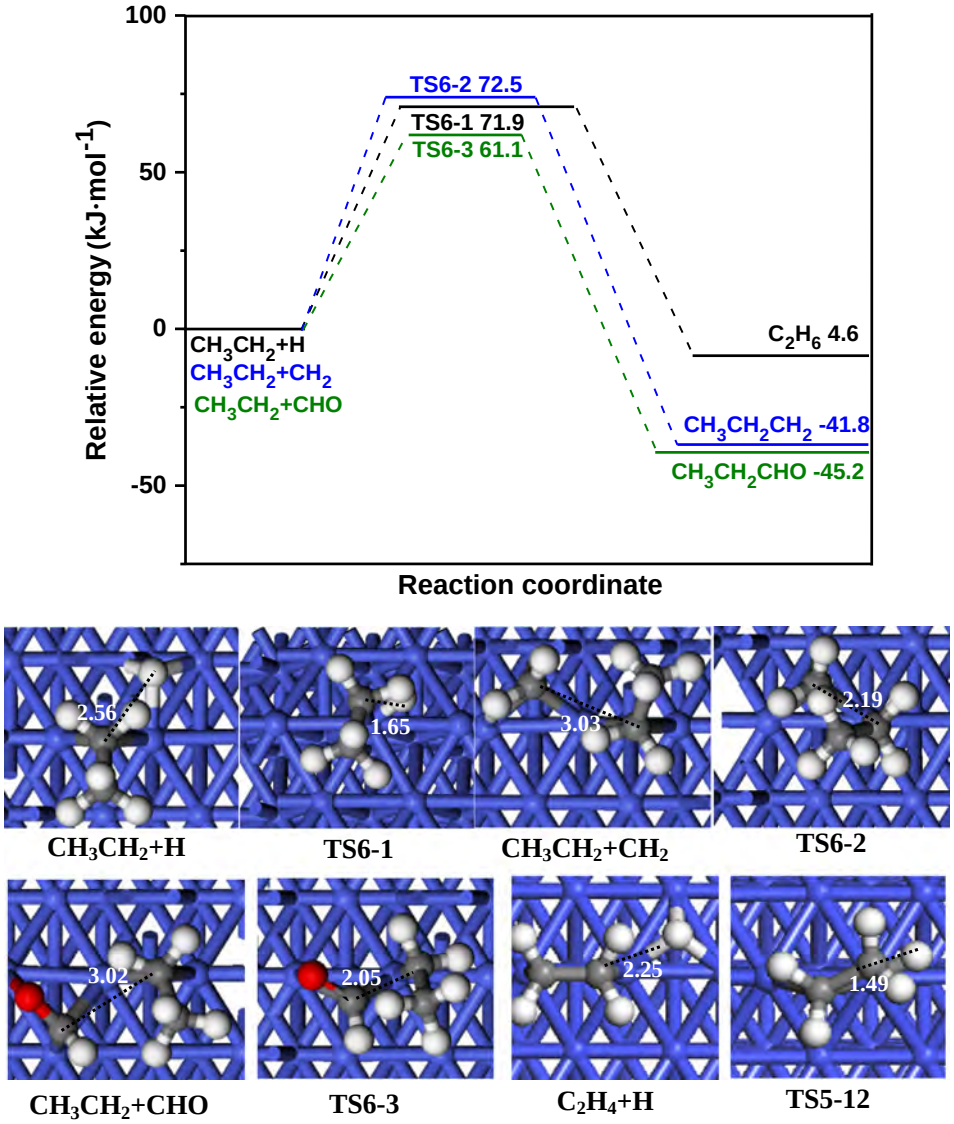

Fig. 10. The potential energy profile of the reactions related to CH_3CH_2 species together with the structures of transition states (TSs) and co-adsorbed species, as well as the structures of ISs and TSs for C_2H_4 hydrogenation on Co(10-10) surface. Other structures are shown in Fig. 2. Bond lengths are in Å.

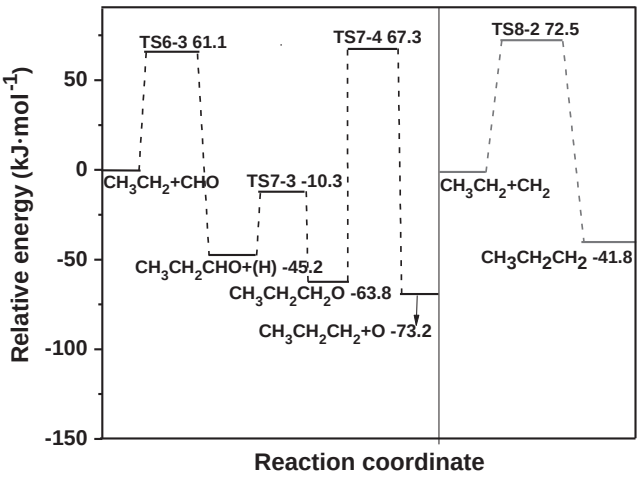

Fig. 11. The optimal potential energy profile of C_3H_x formation via carbide mechanism and CHO insertion mechanism on Co(10-10) surface.

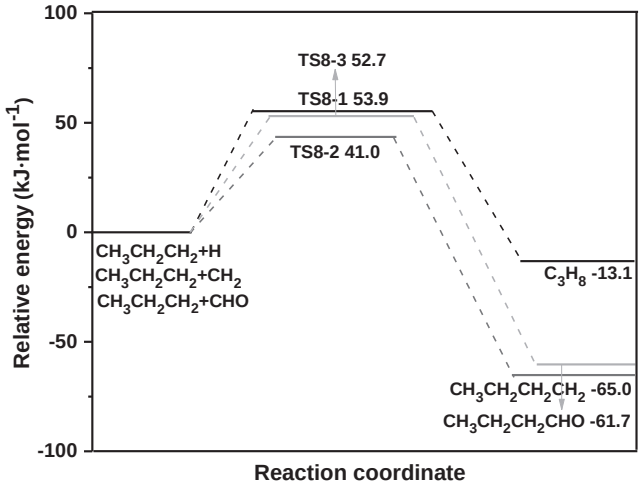

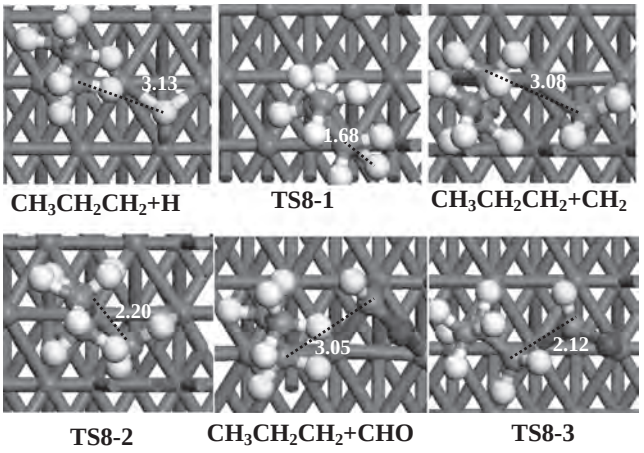

Fig. 13. The potential energy profile of the reactions related to $CH_3CH_2CH_2$ together with the structures of transition states (TSs) and co-adsorbed species on Co(10-10) surface. Other structures are shown in Fig. 2. Bond lengths are in Å.

R'CH_2 can realize the further C—C chain growth. In general, carbide mechanism dominantly contributes to the C—C chain growth of hydrocarbons, and CH_2 is the most favored CH_x monomer to realize the C—C chain growth on Co(10-10) surface. In addition, although CHO insertion into RCH_2 can easily form RCH_2CHO, the thermodynamically instability of CHO limits its interactions with CH_x intermediates; as a result, RCH_2CHO aldehyde oxygenates cannot be easily formed in the product.

3.8. The effect of Hcp Co crystal facets on the preferred mechanism of C—C chain growth

In order to probe into the effect of Hcp Co crystal facets on the preference mechanism of C—C chain growth, the obtained results on Co(10-10) surface in this study are compared with the available results on other Co(0 0 0 1) [27] and Co(10-11) [28] surfaces.

For the favored monomer among CH_x(x = 1–3) species, with respect to CO + H species, on Co(0 0 0 1) surface [27], both CH and CH_2 species are the favored monomer, CH comes from H-assisted CO dissociation (CO + H → CHO → CH + O) with the overall activation barrier of 189.4 kJ mol^{-1}, and CH_2 is from CH hydrogenation; On Co(10-11) surface [28], both CH and CH_2

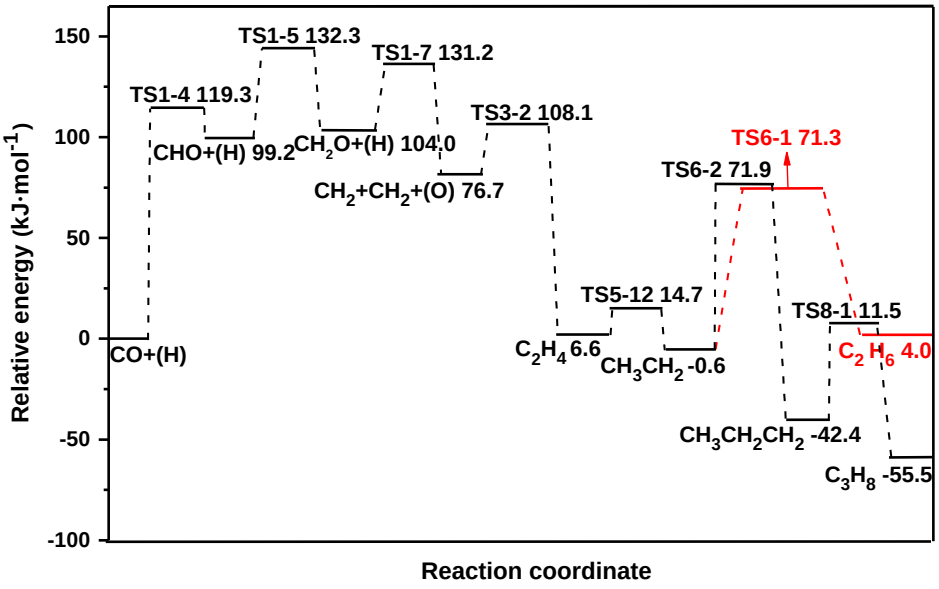

Fig. 12. The potential energy profile for the optimal formation pathways of C_2H_6 and C_3H_8 on Co(10-10).

Table 3
The relative selectivity of all products involving in the C–C chain growth on Co(10-10) surface calculated by microkinetic modeling.

	CH_4	CH_3OH	C_2H_5OH	C_2H_6	C_3H_7OH	C_3H_8
Selectivity (%)	17.72	10.83	0.23	9.56	0.02	61.64

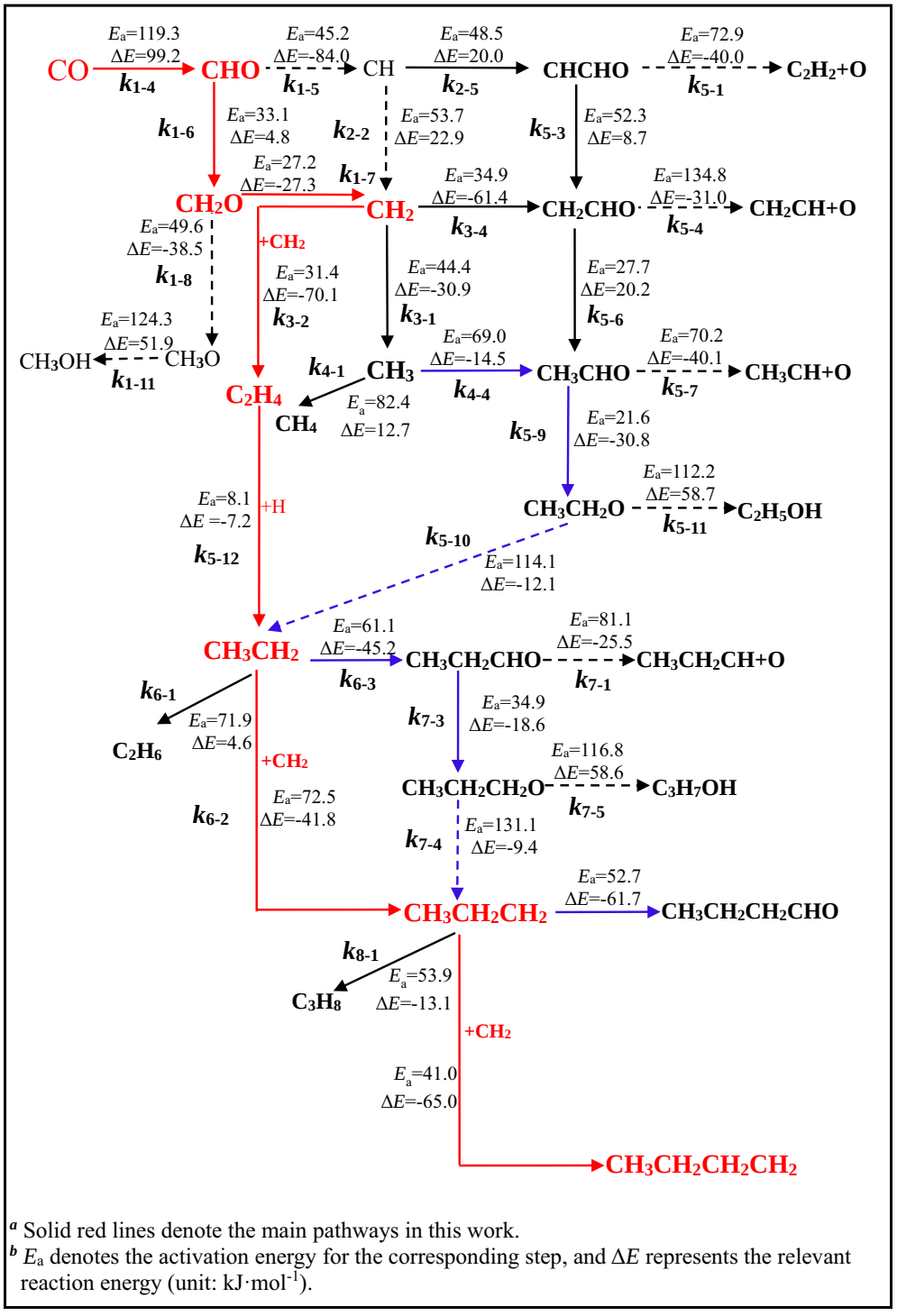

[a] Solid red lines denote the main pathways in this work.
[b] E_a denotes the activation energy for the corresponding step, and ΔE represents the relevant reaction energy (unit: kJ·mol^{-1}).

Fig. 14. Schematic of the optimal reaction pathway for the initiation and growth of C—C chain from syngas on Co(10-10) surface.

species are also the favored monomer, while CH is formed by CO direct dissociation (CO + H → C + O+H → CH + O) with the overall activation barrier of 153.7 kJ·mol^{-1}, and CH_2 is from CH hydrogenation; On Co(10-10) surface in this study, only CH_2 is the favored monomer, which is formed by H-assisted CO dissociation (CO + 2H → CHO + H → CH_2O → CH_2 + O) with the overall activation barrier of 132.3 kJ·mol^{-1}. These results show that the crystal facet of Hcp Co catalyst affects the formation pathway of CH_x species and its favored monomer; moreover, Co(10-10) exhibits the highly catalytic activity towards the formation of favored CH_x

species. Further, since Co(10-11) and Co(10-10) surfaces dominate 63% total surface area exposed of Hcp Co phase [30], the formation of CH_x species over Hcp Co catalyst mainly focus on CO direct dissociation instead of H-assisted CO dissociation.

For the effects of CH_3OH, CH_4 and higher alcohols on Co(0 0 0 1), (10-11) and (10-10) surfaces, CH_x formation is more favorable than CH_3OH, suggesting that these three surface exhibits high selectivity toward CH_x formation, namely, Hcp Co catalyst exhibits high selectivity towards CH_x formation instead of CH_3OH, and CH_3OH has little effects on the production of C_{2+} hydrocarbons. On the other hand, the relative selectivity of CH_4 is 25.53% on Co(10-11) surface, the relative selectivity of CH_4 can reach 17.72% approximately on Co(10-10) surface; whereas the relative selective of CH_4 is low on Co(0 0 0 1) surface compared to other two Co surface; thus, the effect of CH_4 formation on the production of C_{2+} hydrocarbons should be especially considered on Hcp Co catalyst. Further, the relative selectivity of total alcohols over Co(10-11) and (10-10) surfaces can be ignored, namely, Hcp Co catalyst exhibits extremely low selectivity towards total alcohols.

For the preferred mechanism of C—C chain growth, the C—O bond scission of RCH_2CHO and RCHCHO intermediates on Co(0 0 0 1) surface is in favor of the C—C chain growth via CHO insertion mechanism, which is more favorable to realize carbon chain growth *via* the pathway of either $RCH_2CH + CHO \rightarrow RCH_2CHCHO + H \rightarrow RCH_2CH_2CHO \rightarrow R'CH_2CH + O$ or $RCH_2CH + CHO \rightarrow RCH_2CHCHO \rightarrow RCH_2CHCH + H \rightarrow R'CH_2CH$ (R represents H or CH_3, R'=RCH_2). However, on Co(10-11) and (10-10) surfaces, RCH_2CHO and R_2CHCHO prefers to be hydrogenated rather than its C—O bond cleavage, which leads to the C—C chain growth *via* the carbide mechanism, in which RCH_2CH_2 is the dominant intermediate to realize the C—C chain growth of hydrocarbons via the pathway of $RCH_2CH_2 + CH_2 \rightarrow R'CH_2CH_2$ (R'=RCH_2), which is different from that on Co(0 0 0 1) surface *via* CHO insertion mechanism. Thus, the crystal facet of Hcp Co catalyst can affect the preferred mechanism of C—C chain growth.

It is noted that the C—C chain growth *via* CHO insertion mechanism on Co(0 0 0 1) surface [27] showed that CO hydrogenation to CHO at a relatively low coverage is not thermodynamically stable, and therefore the thermodynamically instability of CHO limits its interactions with CH_x intermediates to realize the C—C chain formation [29,62]. Moreover, both Co(10-11) and (10-10) surfaces dominate 63% total surface area exposed of Hcp Co phase [29], as a result, the carbide mechanism should be dominantly responsible for the preferred mechanism of C—C chain growth over Hcp Co catalyst. Further, since the formation of the favored CH_x species is the rate-determining step of C—C chain growth, and Co(10-10) surface exhibits highly catalytic activity towards the formation of the favored CH_x species, thus, Co(10-10) surface exhibits highly catalytic activity towards C—C chain growth among three Co surfaces.

In addition, although the preferred mechanism of C—C chain growth over Co(0 0 0 1), (10-10) and (10-11) surfaces with the corresponding 18%, 28% and 35% total surface area exposed of Hcp Co are investigated, extensive works on other Hcp Co surfaces will be carried out to gain more comprehensive understanding on the C—C chain growth mechanism of Hcp Co, such as the Co(10-12) surface with 12% total surface area exposed of Hcp Co and the stepped surfaces.

4. Conclusions

In summary, the preferred mechanism for the hydrocarbon C—C chain growth in FTS reactions on HCP Co(10-10) surface is obtained using periodic DFT calculations together with microkinetic modeling. The scope of C—C chain growth is limited to the process of $C_1 \rightarrow C_2 \rightarrow C_3 \rightarrow C_4$ hydrocarbons. For the process of $CH_x \rightarrow C_2H_x$, CH_2 self-coupling to C_2H_4, followed by its hydrogenation to CH_3CH_2 leads to C_2 hydrocarbon CH_3CH_2. Then, CH_3CH_2 couples with CH_2 to $CH_3CH_2CH_2$ as the abundant C_3H_x species in the process of $C_2H_x \rightarrow C_3H_x$. Further, $CH_3CH_2CH_2$ couples with CH_2 to $CH_3CH_2CH_2$-CH_2 as the favored C_4H_x species for the process of $C_3H_x \rightarrow C_4H_x$. Therefore, the C—C chain growth on HCP Co(10-10) surface mainly focus on carbide mechanism via CH_2 coupling with alkyl chain instead of C(H)O insertion mechanism. Moreover, the comparisons of the preferred C—C chain growth mechanism among Co(10-10), (10-11) and (0001) surfaces show that the crystal facet of Hcp Co catalyst affects the preferred mechanism of C—C chain growth for hydrocarbons, Co(10-10) surface *via* carbide mechanism is more favorable for the C—C chain growth than Co(0 0 0 1) surface *via* CHO insertion mechanism.

Acknowledgment

This work is financially supported by the National Natural Science Foundation of China (Nos. 21476155, 21736007 and 21776193), the China Scholarship Council, the Program for the Top Young Academic Leaders of Higher Learning Institutions of Shanxi, the Top Young Innovative Talents of Shanxi and U.S. NSF-sponsored NCAR-Wyoming Supercomputing Center (NWSC).

Appendix A. Supplementary material

The detailed descriptions about test results of van der Waals interactions, the adsorption of all possible species, all reactions related to CH_x(x = 1–3), CH_xCHO, CH_3CH_2 and CH_3CH_2CHO species, as well as the calculation method of adsorption energy, activation and reaction energy with zero-point vibrational energy (ZPE) corrections and reaction rate constants, are presented. Supplementary data associated with this article can be found, in the online version, at https://doi.org/10.1016/j.commatsci.2018.01.013.

References

[1] R.E. Ebel, M.P. Croissant, J.R. Masih, International energy outlook: U.S. department of energy, Wash. Q. 19 (1996) 70–99.
[2] H. Schulz, Short history and present trends of Fischer-Tropsch synthesis, Appl. Catal. A: Gen. 186 (1999) 3–12.
[3] M.E. Dry, Practical and theoretical aspects of the catalytic Fischer-Tropsch process, Appl. Catal. A: Gen. 138 (1996) 319–344.
[4] P. Chaumette, P. Courty, A. Kiennemann, B. Ernst, Higher alcohol and paraffin synthesis on cobalt based catalysts: comparison of mechanistic aspects, Top. Catal. 2 (1995) 117–126.
[5] E.D. Mark, The Fischer-Tropsch process: 1950–2000, Catal. Today 71 (2002) 227–241.
[6] A.Y. Khodakov, W. Chu, P. Fongarland, Advances in the development of novel cobalt Fischer-Tropsch catalysts for synthesis of long-chain hydrocarbons and clean fuels, Chem. Rev. 107 (2007) 1692–1744.
[7] G. Jacobs, T.K. Das, Y.Q. Zhang, J.L. Li, G. Racoillet, B.H. Davis, Fischer-Tropsch synthesis: support, loading, and promoter effects on the reducibility of cobalt catalysts, Appl. Catal. A: Gen. 233 (2002) 263–281.
[8] A.Y. Khodakov, Fischer-Tropsch synthesis: relations between structure of cobalt catalysts and their catalytic performance, Catal. Today 144 (2009) 251–257.
[9] E. Iglesia, Design, synthesis, and use of cobalt-based Fischer-Tropsch synthesis catalysts, Appl. Catal. A: Gen. 161 (1997) 59–78.
[10] B.H. Davis, Fischer-Tropsch synthesis: comparison of performances of iron and cobalt catalysts, Ind. Eng. Chem. Res. 46 (2007) 8938–8945.
[11] R.A. van Santen, A.J. Markvoort, I.A. Filot, M.M. Ghouri, E.J. Hensen, Mechanism and microkinetics of the Fischer-Tropsch reaction, Phys. Chem. Chem. Phys. 15 (2013) 17038–17063.
[12] F. Fischer, H. Tropsch, The synthesis of petroleum at atmospheric pressures from gasification products of coal, Brennst. Chem. 7 (1926) 97–104.
[13] R.C. Brady, R. Pettit, Reactions of diazomethane on transition-metal surfaces and their relationship to the mechanism of the Fischer-Tropsch reaction, J. Am. Chem. Soc. 102 (1980) 6181–6182.
[14] Q. Ge, M. Neurock, H.A. Wright, N. Srinivasan, A first principles study of carbon–carbon coupling over the (0001) surfaces of Co and Ru, J. Phys. Chem. B 106 (2002) 2826–2829.

[15] J. Cheng, P. Hu, P. Ellis, S. French, G. Kelly, C.M. Lok, Chain growth mechanism in Fischer-Tropsch synthesis: a DFT study of C–C coupling over Ru, Fe, Rh, and Re Surfaces, J. Phys. Chem. C 112 (2008) 6082–6086.

[16] J. Cheng, X.Q. Gong, P. Hu, C.M. Lok, P. Ellis, S. French, A quantitative determination of reaction mechanisms from density functional theory calculations: Fischer-Tropsch synthesis on flat and stepped cobalt surfaces, J. Catal. 254 (2008) 285–295.

[17] J. Cheng, P. Hu, P. Ellis, S. French, G. Kelly, C.M. Lok, A DFT Study of the chain growth probability in Fischer-Tropsch synthesis, J. Catal. 257 (2008) 221–228.

[18] H. Pichler, H. Schulz, Neuere Erkenntnisse auf dem Gebiet der Synthese von Kohlenwasserstoffen aus CO und H_2, Chem. Ing. Tech. 42 (1970) 1162–1174.

[19] M.K. Zhuo, K.F. Tan, A. Borgna, M. Saeys, Density functional theory study of the CO insertion mechanism for Fischer-Tropsch synthesis over Co catalysts, J. Phys. Chem. C 113 (2009) 8357–8365.

[20] C. Masters, The Fischer-Tropsch reaction, Adv. Organomet. Chem. 17 (1979) 61–103.

[21] M.K. Zhuo, A. Borgna, M. Saeys, Effect of the CO coverage on the Fischer-Tropsch synthesis mechanism on cobalt catalysts, J. Catal. 29 (2013) 217–226.

[22] L.J. Deng, C.F. Huo, X.W. Liu, X.H. Zhao, Y.W. Li, J.G. Wang, H.J. Jiao, Density functional theory study on surface C_xH_y formation from CO activation on Fe_3C (100), J. Phys. Chem. C 114 (2010) 21585–21592.

[23] Y.H. Zhao, K.J. Sun, X.F. Ma, J.X. Liu, D.P. Sun, H.Y. Su, W.X. Li, Carbon chain growth by formyl insertion on rhodium and cobalt catalysts in syngas conversion, Angew. Chem. Int. Ed. 50 (2011) 5335–5338.

[24] G.R. Wang, R.G. Zhang, B.J. Wang, Insight into the preference mechanism for C-C chain formation of C_2 oxygenates and the effect of promoters in syngas conversion over Cu-based catalysts, Appl. Catal. A: Gen. 466 (2013) 77–89.

[25] R.G. Zhang, X.C. Sun, B.J. Wang, Insight into the preference mechanism of CH_x (x = 1–3) and C-C chain formation involved in C_2 oxygenate formation from syngas on the Cu (110) surface, J. Phys. Chem. C 117 (2013) 6594–6606.

[26] X.C. Xu, J.J. Su, P.F. Tian, D.L. Fu, W.W. Dai, W. Mao, W.K. Yuan, J. Xu, Y.F. Han, First-principles study of C_2 oxygenates synthesis directly from syngas over CoCu bimetallic catalysts, J. Phys. Chem. C 119 (2015) 216–227.

[27] G.X. Wen, Q. Wang, R.G. Zhang, D.B. Li, B.J. Wang, Insight into the mechanism about the initiation, growth and termination of the C-C chain in syngas conversion on the Co(0001) surface: a theoretical study, Phys. Chem. Chem. Phys. 18 (2016) 27272–27283.

[28] H.X. Liu, R.G. Zhang, L.X. Ling, Q. Wang, B.J. Wang, D.B. Li, Insight into the preferred formation mechanism of long-chain hydrocarbons in Fischer-Tropsch synthesis on Hcp Co(10–11) surfaces from DFT and microkinetic modeling, Catal. Sci. Technol. 7 (2017) 3758–3776.

[29] J.X. Liu, H.Y. Su, D.P. Sun, B.Y. Zhang, W.X. Li, Crystallographic dependence of CO activation on cobalt catalysts: HCP versus FCC, J. Am. Chem. Soc. 135 (2013) 16284–16287.

[30] G. Kresse, J. Furthmüller, Efficiency of Ab-Initio total energy calculations for metals and semiconductors using a plane-wave basis set, Comput. Mater. Sci. 6 (1996) 15–50.

[31] G. Kresse, J. Furthmüller, Efficient iterative schemes for Ab Initio total-energy calculations using a plane-wave basis set, Phys. Rev. B: Condens. Matter 54 (1996) 11169–11186.

[32] G. Kresse, J. Hafner, Ab Initio molecular dynamics for open-shell transition metals, Phys. Rev. B 48 (1993) 13115–13118.

[33] J.P. Perdew, J.A. Chevary, S.H. Vosko, K.A. Jackson, M.R. Pederson, D.J. Singh, C. Fiolhais, Atoms, molecules, solids, and surfaces: applications of the generalized gradient approximation for exchange and correlation, Phys. Rev. B 46 (1992) 6671–6687.

[34] H.J. Monkhorst, J.D. Pack, Special points for Brillouin-Zone integrations, Phys. Rev. B 13 (1976) 5188–5192.

[35] D. Sheppard, P. H. Xiao, W. Chemelewski, D. D. Johnson, G. Henkelman, A generalized solid-state nudged elastic band method, J. Chem. Phys. 136 2012 074103–1-8.

[36] D. Sheppard, R. Terrell, G. Henkelman, Optimization methods for finding minimum energy paths, J. Chem. Phys. 128 2008 134106–1-10.

[37] G. Henkelman, H. Jónsson, A Dimer method for finding saddle points on high dimensional potential surfaces using only first derivatives, J. Chem. Phys. 111 (1999) 7010–7022.

[38] R.A. Olsen, G.J. Kroes, G. Henkelman, A. Arnaldsson, H. Jónsson, Comparison of methods for finding saddle points without knowledge of the final states, J. Chem. Phys. 121 (2004) 9776–9792.

[39] B.T. Teng, X.D. Wen, M. Fan, Choosing a proper exchange-correlation functional for the computational catalysis on surface, Phys. Chem. Chem. Phys. 16 (2014) 18563–18569.

[40] S. Liu, Y.W. Li, J. Wang, Mechanisms of H_2O and CO_2 formation from surface oxygen reduction on Co (0001), J. Catal. 120 (2016) 19265–19270.

[41] D.R. Lide, Physical and optical properties of minerals, CRC Handbook of Chem. Phys. 4 (1997) 130–136.

[42] M. Ojeda, R. Nabar, A.U. Nilekar, CO activation pathways and the mechanism of Fischer-Tropsch synthesis, J. Catal. 272 (2010) 287–297.

[43] M. Vanin, J.J. Mortensen, A.K. Kelkkanen, J.M. Garcia-Lastra, K.S. Thygesen, K. W. Jacobsen, Graphene on Metals: A van der Waals density functional study, Phys. Rev. B. 81 (2010) 081408–1-4.

[44] S. Grimme, J. Antony, S. Ehrlich, H. Krieg, A consistent and accurate Ab Initio parametrization of density functional dispersion correction (DFT-D) for the 94 elements H-Pu, J. Chem. Phys. 132 (2010) 154104–1-19.

[45] D. C. Sorescu, J. Lee, W. A. Al-Saidi, K. D. Jordan, CO2 adsorption on TiO2(110) rutile: insight from dispersion-corrected density functional theory calculations and scanning tunneling microscopy experiments, J. Chem. Phys. 134 (2011) 104707–1-12.

[46] T. Lu, F.W. Chen, Revealing the nature of intermolecular interaction and configurational preference of the nonpolar molecular dimers $(H_2)_2$, $(N_2)_2$, and $(H_2)(N_2)$, J. Mol. Model. 19 (2013) 5387–5395.

[47] M. Sadeqzadeh, H. Karaca, O.V. Safonova, P. Fongarland, S. Chambrey, P. Roussel, A. Griboval-Constant, M. Lacroix, D. Curulla-Ferré, F. Luck, Identification of the active species in the working alumina-supported cobalt catalyst under various conditions of Fischer-Tropsch synthesis, Catal. Today 164 (2011) 62–67.

[48] M.K. Gnanamani, G. Jacobs, W.D. Shafer, B.H. Davis, Fischer-Tropsch synthesis: activity of metallic phases of cobalt supported on silica, Catal. Today 215 (2013) 13–17.

[49] X.Q. Zhao, S. Veintemillas-Verdaguer, O. Bomati-Miguel, M.P. Morales, H.B. Xu, Thermal history dependence of the crystal structure of Co fine particles, Phys. Rev. B: Condens. Matter 71 (2005) 024106–024112.

[50] X.B. Hao, Q. Wang, D.B. Li, R.G. Zhang, B.J. Wang, The adsorption and dissociation of methane on cobalt surfaces: thermochemistry and reaction barriers, RSC Adv. 4 (2014) 43004–43011.

[51] N.E. Tsakoumis, R. Dehghan, R.E. Johnsen, A. Voronov, W.V. Beek, J.C. Walmsley, B. Øyvind, E. Rytter, D. Chen, M. Rønning, A combined In Situ XAS-XRPD-Raman study of Fischer-Tropsch synthesis over a carbon supported co catalyst, Catal. Today 205 (2013) 86–93.

[52] R.G. Zhang, G.R. Wang, B.J. Wang, Insights into the mechanism of ethanol formation from syngas on cu and an expanded prediction of improved Cu-based catalyst, J. Catal. 305 (2013) 238–255.

[53] W.X. Pan, R. Cao, G.L. Griffin, Direct alcohol synthesis using copper/cobalt catalysts, J. Catal. 114 (1988) 447–456.

[54] L. Joos, I.A.W. Filot, S. Cottenier, E.J.M. Hensen, M. Waroquier, V.V. Speybroeck, R.A.V. Santen, Reactivity of CO on carbon-covered cobalt surfaces in Fischer-Tropsch synthesis, J. Phys. Chem. C 118 (2014) 5317–5327.

[55] J. Yang, Y.Y. Qi, J. Zhu, Y.A. Zhu, D. Chen, A. Holmen, Reaction mechanism of CO activation and methane formation on Co Fischer-Tropsch catalyst: a combined DFT, transient, and steady-state kinetic modeling, J. Catal. 308 (2013) 37–49.

[56] M. Lindroos, C.J. Barnes, P. Hu, D.A. King, The termination and multilayer relaxation at the Co (1010) surface, Chem. Phys. Lett. 173 (1990) 92–96.

[57] H. Over, G. Kleinle, G. Ertl, W. Moritz, K.H. Ernst, H. Wohlgemuth, K. Christmann, E. Schwarz, A LEED structural analysis of the Co(1010) surface, Surf. Sci. 254 (1991) L469–L474.

[58] G.T.K.K. Gunasooriya, A.P. Van Bavel, H.P.C.E. Kuipers, Key Role of surface hydroxyl groups in C-O activation during Fischer-Tropsch synthesis, ACS Catal. 6 (2016) 3660–3664.

[59] S. Liu, Y.W. Li, J. Wang, Mechanisms of H-and OH-assisted CO activation as well as C-C coupling on the flat Co (0001) surface-revisited, Catal. Sci. Technol. 6 (2016) 8336–8343.

[60] R.G. Zhang, F. Liu, Q. Wang, B.J. Wang, D.B. Li, Insight into CH_x formation in Fischer-Tropsch synthesis on the hexahedron Co catalyst: effect of surface structure on the preferential mechanism and existence form, Appl. Catal. A: Gen. 525 (2016) 76–84.

[61] S. Eckle, H.G. Anfang, R.J. Behm, Reaction intermediates and side products in the methanation of CO and CO_2 over supported Ru catalysts in H_2-rich reformate gases, J. Phys. Chem. C 115 (2010) 1361–1367.

[62] O.R. Inderwildi, S.J. Jenkins, D.A. King, Fischer-Tropsch mechanism revisited: alternative pathways for the production of higher hydrocarbons from synthesis gas, J. Phys. Chem. C 112 (2008) 1305–1307.

[63] J. Cheng, P. Hu, P. Ellis, S. French, G. Kelly, C.M. Lok, A first-principles study of oxygenates on Co surfaces in Fischer-Tropsch synthesis, J. Phys. Chem. C 112 (2008) 9464–9473.

[64] N. Kapur, J. Hyun, B. Shan, J.B. Nicholas, K. Cho, Ab Initio study of CO hydrogenation to oxygenates on reduced Rh terraces and stepped surfaces, J. Phys. Chem. C 114 (2010) 10171–10182.

[65] O.R. Inderwildi, D.A. King, S.J. Jenkins, Fischer-Tropsch synthesis of liquid fuels: learning lessons from homogeneous catalysis, Phys. Chem. Chem. Phys. 11 (2009) 11110–11112.

[66] P. Liu, A. Logadottir, J.K. Nørskov, Modeling the electro-oxidation of CO and H_2/CO on Pt, Ru, PtRu and Pt_3Sn, Electrochim. Acta. 48 (2003) 3731–3742.

[67] L. Barrio, P. Liu, J.A. Rodriguez, Effects of hydrogen on the reactivity of O2 toward gold nanoparticles and surfaces, J. Chem. Phys. 126 (2007) 164705–1-8.

[68] P. Liu, J.A. Rodriguez, Water-gas-shift reaction on metal nanoparticles and surfaces, J. Phys. Chem. B 110 (2006) 19418–19425.

[69] Y.M. Choi, P. Liu, Mechanism of ethanol synthesis from syngas on Rh (111), J. Am. Chem. Soc. 131 (2009) 13054–13061.